Spring 5-2018

Intra-Annual Fjord Circulation: Seasonal Variation in Fjord Physics and Biology and the Impacts of a Glacial Lake Outburst Flood

Brigitte E. Parady
University of Maine

INTRA-ANNUAL FJORD CIRCULATION: SEASONAL VARIATION IN FJORD PHYSICS AND BIOLOGY AND THE IMPACTS OF A GLACIAL LAKE OUTBURST FLOOD

by

Brigitte E. Parady

A Thesis Submitted in Partial Fulfillment
of the Requirements for a Degree with Honors
(Civil and Environmental Engineering)

The Honors College

University of Maine

May 2018

Advisory Committee:

Lauren Ross, Assistant Professor of Civil and Environmental Engineering, Advisor
Kimberly Huguenard, Assistant Professor of Civil and Environmental Engineering
Neil R. Fisher, Civil and Environmental Engineering Lab Manager
Jean MacRae, Professor of Civil and Environmental Engineering
Edith Elwood, Professor of English, Honors College

ABSTRACT

Climate change is expected to significantly affect the world's fjords by increasing storm intensity and glacial lake outburst floods (GLOFs). GLOFs are characterized as a sudden release of glacial trapped waters into a fjord, yet how they modify fjord circulation and zooplankton migration patterns is not well understood. This study aims to investigate long-term physical and biological patterns in fjords and how they are modified by GLOFs by characterizing intra-annual variation in fjord hydrodynamics and biology. The study area is Martinez Channel in Chilean Patagonia located below the Northern Patagonia Ice Field. To accomplish this goal, circulation patterns and temporal and spatial variations of zooplankton will be analyzed in the presence of a GLOF and under normal conditions. The data collected include horizontal current velocities measured throughout the water column with a moored (~80 m depth), upward facing, acoustic doppler current profiler (ADCP) which sampled hourly in 1 m vertical bins. Salinity, temperature, wind, and river discharge data were also analyzed to complement the velocity measurements. Results showed that the baroclinic annular mode (BAM), a proxy for storminess in the Southern Hemisphere, significantly influenced the fjord every ~20-30 days. The BAM induced mixing which caused pycnocline depressions that interacted with the diel vertical migration of zooplankton. The strong winds associated with the BAM were also enough to retain floodwaters from the GLOF in early February. This study proves that external events such as the BAM and GLOFs affect fjord physics and biology and should be considered in future studies.

DEDICATION

I would like to dedicate this thesis herein to Faith P. Kenney without whom I would not be able to accomplish this thesis and my subsequent graduation. Her role in fostering critical thinking throughout my childhood led me to grow into a successful and intellectual person and I am forever grateful.

ACKNOWLEDGEMENTS

I would first and foremost like to thank my thesis advisor, Dr. Lauren Ross, for the effort she put forth to shape this thesis into an excellent final product. Her dedication and patience were what allowed me to excel and her intelligence on the subject supported me in my research. I would secondly like to thank Dr. Leonardo Castro and COPAS Sur-Austral project for funding the research that provided my data. I would lastly like to thank all committee members for their willingness to be present as a support system during this process. Additional people who positively influenced the outcome of this thesis include Dr. Ivan Perez-Santos, Ally Redcay, Dr. Neil Fisher, Dr. Kimberly Huguenard, Dr. Andrew Thomas, and Dr. Mark L. Wells. Without these individuals this project would not have been possible.

TABLE OF CONTENTS

LIST OF FIGURES

INTRODUCTION

The inevitability of climate change has prompted interest in understanding how Earth's systems respond to a warming atmosphere. One major consequence of climate change is the melting of glaciers and icefields, leading to sea level rise. In particular, oceans have risen 4 to 8 inches over the past century with an annual rise of 0.13 inches per year (Warne, 2017). Icefields and glaciers have recently experienced more rapid melting (Chen et al., 2010; Glick, 2017; Harrison et al., 2006, and references therein; Somos-Valenzuela et al., 2016), accelerating sea level rise. In Chilean Patagonia, glaciers are reacting dynamically to climate change (Harrison et al., 2006). Specifically, in the Northern Patagonia Icefield, Steffen glacier has lost 12 km^2, Glaciares Nef has lost 7.9 km^2, and nearby Colonia glacier has lost 9.1 km^2 of surface area since 1979 (Rivera et al., 2007). This extreme melting first affects local water bodies, which includes fjords, and subsequently the world's oceans.

Fjords are glacially carved channels located in high-latitude regions where glacial activity is (active glacier) or was (extinct glacier) prevalent (Valle-Levinson, 2010). Generally, fjords are long, narrow, and deep with a typical width-depth ratio of 10:1 (Dyer, 1997; Farmer and Freeland, 1983) and a sill (or moraine) is typically located at the mouth of the fjord where it connects to the open ocean (Dyer, 1997; Farmer and Freeland, 1983). Fjords are characterized by their strong salinity-driven stratification with a thin buoyant layer at the surface (~0 g/kg) derived from glacial melt, river discharge, precipitation, and coastal runoff (Farmer and Freeland, 1983; Inall and Gillibrand, 2010; Pantoja et al.,

2011) overlying a salty dense layer below (~35 g/kg). Mixing between layers results from inflowing saltwater and outflowing freshwater generating shear between the two layers or from internal waves and tides (Inall and Gillibrand, 2010). The divide between saltwater and freshwater is referred to as the halocline and represents a sharp increase in salinity over a small portion of the total depth as illustrated in figure 1.1 (Farmer and Freeland, 1983). A sharp increase in density with depth is called the pycnocline, and in fjords this density change is driven by vertical variations in salinity (halocline) more than temperature (thermocline).

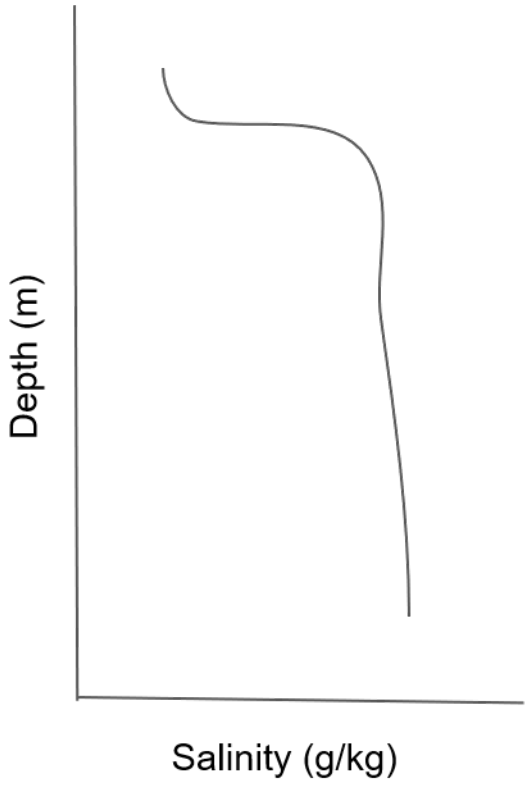

Figure 1.1: A typical density profile in a fjord (based on descriptions from Dyer, 1997).

Ultimately, climate change will alter the above-mentioned water column properties and biology of fjord systems (Aiken, 2012; Marín et al., 2013). In particular, temperature, salinity, and circulation structure will be impacted by rising ocean and atmospheric

temperatures and glacial lake outburst floods (GLOFs) and, in turn, biology will be affected by these altered properties. As a result of increased temperatures and ice melt, the frequency and intensity of GLOFs has become elevated (Dussaillant, 2009; Harrison et al., 2005; Ross et al., 2015). GLOFs occur as a result of water trapped by a glacial dam suddenly being released due to the dam melting. In particular, water from the nearby glacially fed lake penetrates the ice dam when air temperatures rise, which causes a sudden release of meltwater at high flow rates (Dussaillant, 2009; Palmer, 2017). These floodwaters often travel through fjords and impact local properties and biology. This release has the potential to be devastating. For example, a 1941 GLOF in Peru killed 500 people (Somos-Valenzuela, 2016).

Glacial melting in Chilean Patagonia is significant in comparison with the rest of the world (Marín et al., 2013). An estimated 10% of sea-level rise over the past 50 years can be attributed to the Patagonian Icefield glaciers (Glasser et al., 2011). Therefore, significant freshwater inputs can be expected in Patagonian fjords which could affect fjord stratification. A primary driver of vertical mixing in fjords is internal waves and tides that are influenced by the barotropic tide. The barotropic tide represents a long wave that is forced by the gravitational pull from the moon and sun (Dushaw, 2003). Turbulence is induced when the ocean tide interacts with fjord bathymetry and subsequently mixes the interface between fresh and saltwater. Fjords have characteristically varying bathymetry due to the presence of multiple sills and constrictions, which provide desirable conditions for vertical mixing. Increased discharge

of freshwater into the fjord due to glacial melt could enhance stratification and inhibit mixing induced by the barotropic tide.

The barotropic tide can also interact with river plumes. Ross et al., (2014) investigated the role of internal waves resulting from interactions between the barotropic tide and discharge from a river plume. This interaction occurs in estuaries when the Froude number, a nondimensional number defined as the ratio of the ambient flow velocity to the wave speed, is greater than 1, indicating supercritical flow. This flow condition prevents waves from propagating upstream and indicates that internal waves with horizontally propagating wave energy are likely generated by tidal interactions with a river plume (Ross et al., 2014). In particular, when horizontal velocities converge at the plume (during flood tide), it causes frontal growth and a downward displacement of surface waters. In other words, when the propagation speed at the river plume front is less than the tidal wave speed (the water in front of the plume), this causes a depression of the pycnocline by forcing freshwater downwards and once the tide turns (ebb tide) internal waves are free to propagate out-fjord (as the Froude number drops below 1) (Nash and Moum, 2005). Ross et al., (2014) found correlation between pulses in river discharge with pulses of internal tides near the pycnocline in a Patagonian fjord. Her study indicated that river discharge pulses exceeding 1200 m^3/s caused a vertical displacement of the pycnocline between ~10-20 m that contributed to vertical mixing of both physical and biochemical water properties (Ross et al., 2014). Deepening of the buoyant, fresh water layer at the surface of the fjord due to glacial melt and GLOFs will alter internal

wave/tide behavior and interfacial mixing in the fjord, which can then alter the circulation.

Specifically, changes in precipitation and glacial melt associated with climate change are expected to impact the driving forces of circulation in Chilean Patagonian fjords (Aiken, 2012; Fuenzalida et al., 2007). It is important to understand changes in circulation in order to make predictions for future fjord conditions under a different climate. Recent increases in GLOF events has also urged investigation into how these events affect fjord systems in terms of circulation and biology. Marín et al., (2013) found that the Baker River, one of the largest rivers in Chile in terms of discharge values, experienced a 600% increase in GLOF events between 2010 and 2012. This affects circulation patterns in Baker and Martinez Channels, since both fjords receive the discharge from the Baker River. As for the biological activity in the fjords, variations in precipitation and freshwater discharge affect primary and secondary production (Pantoja et al., 2011). Secondary production such as zooplankton rely on primary production as a main food source. Primary production includes phytoplankton which require freshwater and sunlight to live (Montecino et al., 2008). In particular, increased light attenuation attributed to elevated suspended sediments during a GLOF event can adversely impact phytoplankton and zooplankton production (Ross et al., 2015).

Studies linking zooplankton to fjord circulation are limited, especially in Chilean Patagonia. However, studies indicate that stratification in fjords contributes to spatial distributions of zooplankton (Meerhoff et al., 2014). More specifically, phytoplankton (referred to as primary producers) dwell in the less saline surface waters and zooplankton

ascend from depth to feed on them. This vertical migration pattern is often regulated by light availability. Influxes of sediments and freshwater due to GLOFs can enhance light attenuation and alter the vertical migration pattern of the zooplankton as well as temporarily enhance gravitational circulation patterns in a fjord (Alldredge and King, 1980; Valle-Levinson et al., 2014).

How circulation patterns in Chilean Fjords vary on seasonal and annual temporal scales is not yet well understood. The hydrographic properties of fjords drive circulation patterns, which in turn impacts local biology. It is important to investigate intra-annual variations in order to assess how fjords will be altered by climate change. The main goal of this study is to determine how the circulation of a glacial fjord in Chilean Patagonia varies throughout a year by addressing two research objectives. The first objective is to characterize how the hydrodynamics of the fjord vary intra-annually and in the presence of a GLOF. The second objective is to assess how the hydrodynamics of the fjord links to the biology by characterizing temporal variations of zooplankton distributions throughout the water column.

The research objectives will be met using a unique, one-of-a-kind dataset from a Chilean Patagonian Fjord. In particular, it is the first to encompass data from the majority of the water column for a full year in this region. This has never before been accomplished due to the harsh weather conditions and rural location of most Chilean fjords that complicate data sampling. This study is unique in the use of river discharge data as well as wind, density, current velocity, echo anomaly (and volume backscatter as a proxy for

zooplankton distributions), to explain the water column properties, circulation and variations in zooplankton in the fjord for an entire year. These data were processed using various data analysis techniques such as echo anomaly, lowpass filtering, spectral analysis, and empirical orthogonal function (EOF) analysis.

The remainder of this paper will include an explanation of the study area in Section 2 followed by the methods used, including data collection and data analysis in Section 3. The results will be presented in Section 4 and discussed in Section 5. Study limitations will be addressed in Section 6 and conclusions will be presented in Section 7.

STUDY AREA

Located in the Southern Hemisphere, Patagonian Chile represents 240,000 km^2 of glacially carved land on the southwest coast of Chile (encompassing ~1000 km in a straight line) (Pantoja et al., 2011). Its geography is composed of mountainous coastline and complex fjord and channel systems that were glacially carved through the steep slopes of the Andes mountain range. The Northern and Southern Patagonia Ice Fields supply freshwater to the fjords through glacially fed rivers and lakes. These ice fields represent the largest two bodies of ice in the southern hemisphere (Ross et al., 2015).

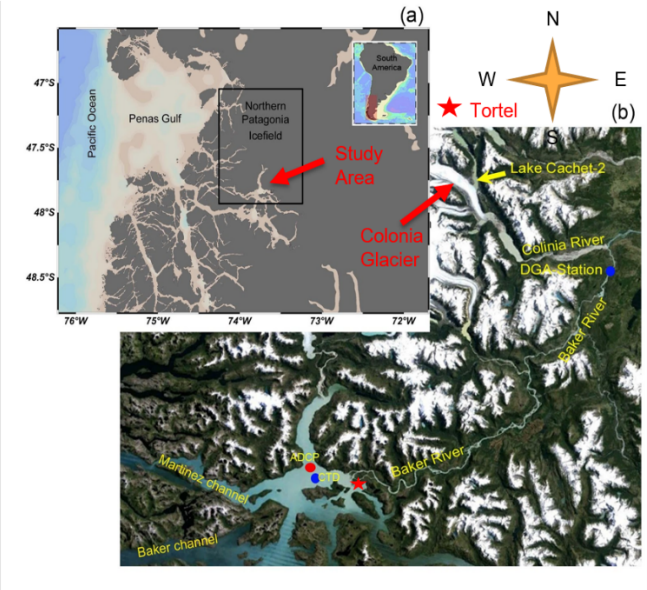

Figure 2.1: (a) geographical location of study area and (b) closer picture of the study area including ADCP mooring station, CTD casting area, DGA river collection station. Lake Cachet 2, which drains through Colonia Glacier, is also identified as well as the village of Tortel that is particularly vulnerable during GLOF events (figure adapted from Ross et al., (2015)).

The study area is located towards the bottom of the Northern Patagonian Ice Field. Glacial runoff of Colonia Glacier, seen in figure 2.1, follows Colonia and Baker Rivers through the Baker-Pascua Estuary (BPE) system into the open ocean. The BPE is a complex fjord system comprised of Baker and Martinez channels, the latter of which is focused on in this study. Between 200 and 440 m deep, Martinez Channel is oriented

with the along-channel axis in the East-West direction and this system experiences primarily semi-diurnal tides (~1 m amplitude and period of 12.42 h) (Piret et al., 2017; Ross et al., 2014). The mouth of Martinez channel (3.5 km wide) connects to the open ocean ~100 km from the head of the system (Ross et al., 2015). Baker Channel also makes a connection with the open ocean ~100 km from the system's head with its mouth (5 km wide) connecting further south than the mouth of Martinez Channel (Ross et al., 2015). Typical wind influence in this area is shown in figure 2.2.

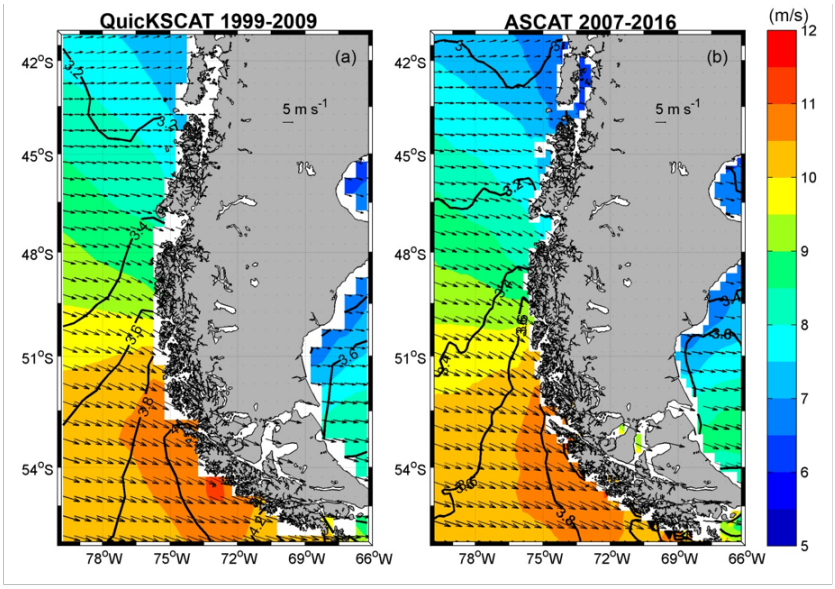

Figure 2.2: Typical wind influence in the study region.

Freshwater in Martinez Channel is primarily derived from the Baker River with average annual discharge exceeding 1100 $m^3 s^{-1}$ (Ross et al., 2015). The freshwater layer is about 5-10 m deep with low temperatures (< 8 ˚C) and low salinity (< 30 g/kg; Ross et al., 2014; Ross et al., 2015). Upstream, Colonia glacier forms an ice dam preventing water from Lake Cachet 2 (surface area of 4 km^2) from flowing into the Baker River (Marín et al., 2013) (figure 2.3). Long-term thinning of this Colonia glacier has led to an increase in Glacial Lake Outburst Flood events (Casassa et al., 2010). During a GLOF, meltwater

bursts through Colonia Glacier via an englacial tunnel running 8 km in length (Casassa et al., 2010). From there, it flows through Colonia Lake and the confluence between Colonia and Baker Rivers into Baker and Martinez channels. The village of Tortel at the mouth of Baker River is particularly vulnerable to damage during a GLOF due to its location (figure 2.1). Primary transportation in Tortel consists of walkways constructed along the coast which are susceptible to destruction during flooding.

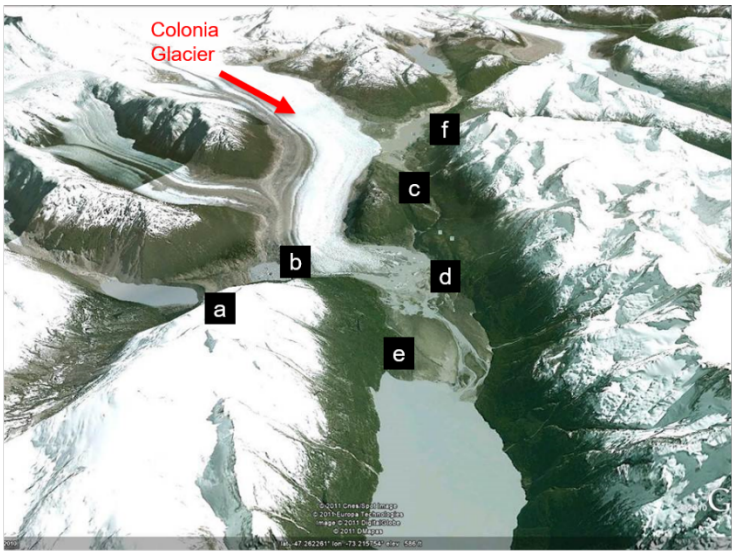

Figure 2.2: Colonia glacier which feeds into (a) Arco Lake, (b) East Terminal Lake, (c) Lake Cachet 1, (d) West Terminal Lake, (e) Colonia Lake which feeds into Colonia River and subsequently Baker River, and (f) Lake Cachet-2 (figure adapted from glacierchange.wordpress.com)

METHODS

3.1 Data Collection

The remote location of this study area provides limitations to the type and extent of data collection that can occur. This study recognizes that there might be limitations on conclusions that can be drawn, especially because there is no data representing meltwater runoff from the nearby Steffen Glacier. Nonetheless, the data provided in various locations in Martinez Channel and Baker River allowed for a variety of analyses to be performed.

Hydrographic data including temperature, salinity, density, chlorophyll, and dissolved oxygen were collected in Martinez Channel using a SeaBird Electronics 19 plus Conductivity, Temperature, Depth (CTD) profiler. Vertical casts ~100 m deep were collected at the junction between Martinez Channel and Steffen Fjord (figure 2.1; 46.82167°S 73.62167°W). CTD casts were taken in January, June, November, and December of 2014. These measurements display an overview of hydrographic properties of the fjord in the austral (southern hemisphere) seasons.

Hourly river discharge data was provided by the Chilean Water Directorate from Colonia station referred to as DGA station in figure 2.1 (47.5009 °S, 72.9749 °W). These data provide an overview of the discharge values throughout 2014. According to Marín et al., (2013) and Ross et al., (2015), a discharge value above 2000 m^3/s represents a GLOF. Wind data were recorded every three hours from a Chilean navy lighthouse in Penas Gulf

(figure 3.1; 46.82167°S, 73.62167°W). As these data were collected outside of the immediate study area, they are intended to give a representative portrayal of the wind regime in the area.

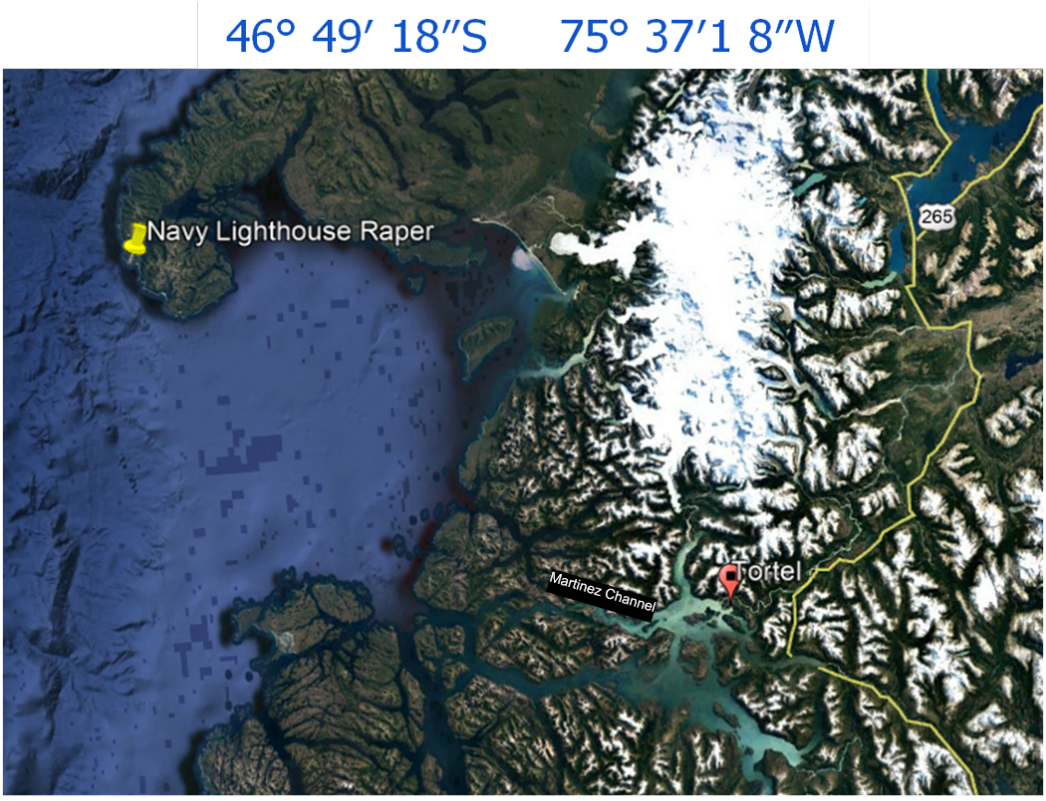

Figure 3.1: Navy Lighthouse shown in proximity to Martinez Channel and the village of Tortel (image from Google Maps).

Backscatter and current velocity data were collected using a 307.2 kHz Teledyne RDI workhorse Acoustic Doppler Current Profiler (ADCP) moored ~6.2 km to the west of the Baker River mouth (73.73 °W, 47.82 °S) and ~85 km downstream of DGA station. The ADCP was moored at the junction between Martinez Channel and Stefan Fjord (figure 2.1). The ADCP was moored facing upwards at 86 m depth from January 28th-June 11th, at 82 m depth from June 11th-December 17th, and at 96 m depth from December 17th-December 28th, encompassing nearly the full year of 2014. Measurements were collected

in 1 m vertical bins every hour with pings sent every 14.4 seconds and 250 pings per ensemble average.

3.2 Data Analysis

3.2.1 Buoyancy Frequency

Buoyancy frequency (or Brunt–Väisälä frequency), denoted N^2, represents the oscillating frequency of a vertically displaced particle within a statically stable environment and can be used as a proxy for stratification (Emery and Thompson, 2014). The highest buoyancy frequency values are shown at depths with the most pronounced changes of density (i.e. the pycnocline). The buoyancy frequency is calculated from density as:

$$N^2 = \frac{-g}{\rho_0}\frac{\partial \rho}{\partial z} \qquad (3.2.1.1)$$

where N^2 is the buoyancy frequency, g represents gravitational acceleration, ρ_0 represents a reference density in the water column and $\frac{\partial \rho}{\partial z}$ represents the gradient of the water density, ρ, with respect to depth, z.

In this study, buoyancy frequency was calculated for the summer and winter CTD casts using density recorded over depth. To perform the analysis, the density gradient of each cast is multiplied by the negative of gravity divided by the mean density. The buoyancy frequency was used to determine the depth of the pycnocline in the fjord for various seasons.

3.2.2 Backscatter and Echo Anomaly

Backscatter is a measure of sound scatter off of particles suspended in the water column. The ADCP uses the backscatter to measure the velocity in the water column from the Doppler shift. The backscatter can include elevated values close to the ADCP due to

feedback associated with particles in close proximity. The echo anomaly is calculated to normalize the backscatter and remove the feedback associated with particles near the ADCP (removed attenuation of the backscatter). This is done with the following formula:

$$EA = 10\log_{10}(ECHO) - <10\log_{10}(ECHO)> \quad (3.2.2.1)$$

where *EA* is echo anomaly, *ECHO* represents backscatter from the ADCP, and the angle brackets denote a time mean over the entire time series (January 28th-December 27th, 2014; Ross et al., 2014; Valle-Levinson et al., 2004). Backscatter is measured by the ADCP sending out a sound ping that returns to the device after bouncing off a 'scatterer' in the water column. Therefore, the *EA* shows the intensity of scatterers throughout the water column such as zooplankton, suspended sediments, detritus, and density gradients. It can also be useful in exploring biological and sediment activity during a GLOF (Cabrer, 1987). The *EA* picks up on density interfaces (air/sea, water/bottom) and therefore can also be used as a proxy for pycnocline location, which can be verified by the buoyancy frequency values (Ross et al., 2014; Valle Levinson et al., 2004). In this study, *EA* was particularly relevant in exploring vertical patterns found throughout the water column and during various seasons in Martinez Channel, which are hypothesized to be the diel vertical migrations (DVM) of zooplankton. This involves zooplankton migrating up to the pycnocline and back to depth between sunset and sunrise. In order to separate out zooplankton from the scatterers found in the *EA*, the volume backscatter (*Sv*) was investigated.

3.2.3 Volume Backscattering Strength

Volume backscatter (*Sv*) is another analysis tool derived from backscatter. It can be used as a proxy for zooplankton concentrations in the water column by effectively removing

particles with diameter less than ~5 mm based on the 307.2 kHz ADCP used (Greene and Wiebe, 1990; Ross et al., 2015). This limiting diameter was found using equation (3.2.3.1) as shown in Valle Levinson et al., (2014) who studied a fjord using an ADCP with the same frequency used in this study:

$$\lambda = \frac{c}{f} = \frac{1500\ m/s}{307000\ Hz} = 4.9\ mm \qquad (3.2.3.1)$$

where c represents the speed of sound in water, f is the ADCP frequency in Hz, and λ is the size of detectable plankton (Postel et al., 2007). The volume backscatter was calculated with the following equation:

$$Sv = C + 10 * log\ [(T_x + 273.16)R^2]\ - L_{DBW} - P_{DBW} + 2\gamma R + K_C(E - E_r) \qquad (3.2.3.2)$$

where C is -148.2 dB for the Workhorse Sentinel ADCP and represents a sonar-configuration scaling factor. T_x is the temperature recorded at the ADCP in °C throughout the data collection period. L_{DBW} is 10*$\log_{10}$(transmit-pulse length in meters) where the transmit-pulse length is 8.13 m. P_{DBW} is 10*$\log_{10}$(transmit power in W) and was found to be 15.5 W based on the ADCP frequency. The absorption coefficient is represented by γ= 0.001 dB m^{-1}. K_c was given by the manufacturer as 0.45 and represents a beam-specific sensitivity coefficient. E is the recorded backscatter throughout the water column over time and E_r is the minimum recorded backscatter (38 dB in this study). R is calculated through the following equation:

$$R = \frac{b + \frac{L+d}{2} + ((n-1)d) + (\frac{d}{4})}{cos\xi} * \frac{\bar{c}}{c_I} \qquad (3.2.3.3)$$

Where b is blanking distance (3.23 m) and L is the previously defined transmit pulse length (8.13 m). The depth cell length (1 m) is defined by d, n is an index of the depth cells, and the beam angle (20 °) is represented by ξ. Average sound speed from the

transducer to the depth cells (1453 m/s) is represented by $\bar{c}$ and the speed of sound used by the instrument (1454 m/s) is represented by c_I.

To understand the dominant periodicity found in the current velocities, *EA* and *Sv*, a spectral analysis was adopted.

3.2.4 Spectral Analysis

Spectral analysis (also denoted as power spectra) is the square of the fast Fourier transform of the data. The Fourier transform decomposes finite sets of time varying data into dominant frequencies by breaking them into orthogonal components. Spectral analysis was applied to the echo anomaly to determine what frequencies (in cycles per day) harbored the highest energy. Spectral analysis displays the frequencies (in cpd) within a time series that contain the most energy. It can be used to determine the cycles (frequencies) with greatest influence on fjord variability. For example, high energy in the spectra of the echo anomaly is typically found at tidal and subtidal time scales and has been used to reveal diel vertical migrations (DVM) of zooplankton (Ross et al., 2015; Valle-Levinson et al., 2014).

Parameters used in a spectral analysis involve window size and type of window used. This study used a Hanning Window (named after Austrian meteorologist Julius von Hann) which represents a Gaussian Curve spanning a defined window size that is defined by 2^n where *n* is a number that yields a window size less than the sample size (*n*=11; window size of 2048; sample size of 8003 in this study). Figure 3.2.4.1 shows the window used in the spectral analysis performed in this study. The number of windows applied to the echo anomaly was based on the length of the time series.

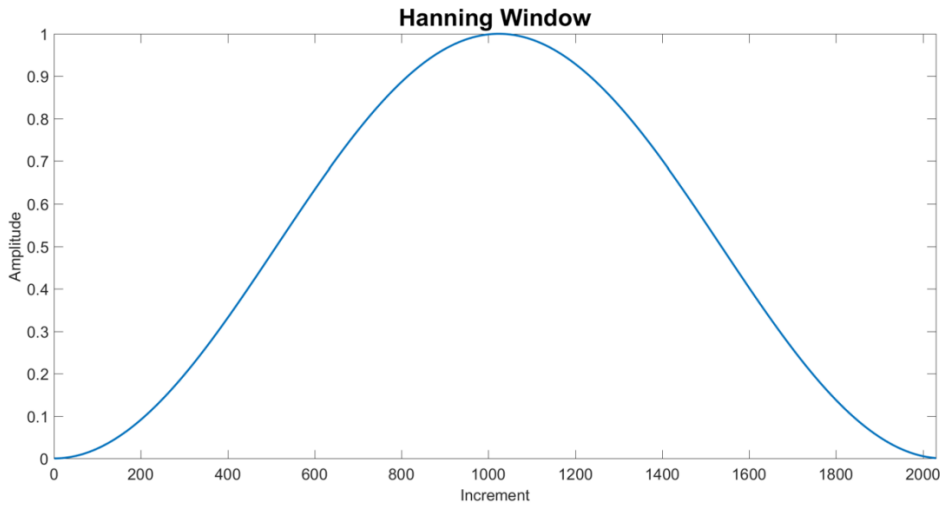

Figure 3.2.4.1: Hanning Window of size 2048 used in spectral analysis. Increment represents the location in the time series and amplitude is what the data at that corresponding increment is multiplied by to normalize it.

A spectral analysis was calculated for each individual window and summed to produce a final spectra for the whole time series. This was done by sectioning the echo anomaly by window size and multiplying by the Hanning Window. The fast fourier transform (*fft*) of this product was then squared and multiplied by the square root of 8/3 to achieve the spectra of that window. Equation 3.2.4.1 shows this calculation where *specW* is the spectra of the desired window, *w* is the Hanning Window, *EA* is the echo anomaly from *ll* to *lu* which represent the beginning and end of the window respectively:

$$specW = \sqrt{8/3} * fft(w * EA(ll{:}\, lu)^2) \qquad (3.2.4.1)$$

To obtain the power spectra for the entire data set at each depth, the spectra were visualized with respect to the frequency vector and depth. Spectral analysis allows for the determination of dominant frequencies of variability in the fjord system. However, it does not describe dominant spatial patterns. To quantify the dominant modes of both spatial and temporal variability, Empirical Orthogonal Function (EOF) Analysis was utilized.

3.2.5 Empirical Orthogonal Function Analysis (EOF)

Empirical Orthogonal Function Analysis decomposes a spatially and temporally varying data set into multiple orthogonal functions representing dominant modes of variability. The dominant mode, denoted M1, explains the majority of the variability, M2 the second most and so on until 100% of the variance is explained. For the application of EOF analysis conducted on the echo anomaly in this study, the spatial variability displays the modal range throughout the fjord depth.

Echo anomaly varies spatially with depth over a given time series. For the purpose of this analysis, it will be represented as $u_n(t_m)$ where n represents the spatial interval from $1<n<110$ (since there are 110 ADCP depth bins) and m is the time interval in hours from $1<m<M$ where M is the last measurement recorded from the ADCP (~8003 measurements). In order to apply an EOF analysis to the echo anomaly, the spatial components that vary with depth must be expressed as the sum of n orthogonal spatial functions (Ross et al., 2014). These functions are denoted $\alpha_i(z_n)=\alpha_{in}$ and used to calculate $u_n(t_m)$ through the following equation:

$$u_n(t_m)= \sum_{i=1}^{n}[\alpha_i(t_m)\ \alpha_{in}] \qquad (3.2.5.1)$$

where $\alpha_i(t_m)$ represents the amplitude of the ith orthogonal mode at time t_m (Emery and Thomson, 2004; Kaihatu et al., 1998; Ross et al., 2014). Temporal variation of spatial modes α_{in} is shown by the time amplitude $\alpha_i(t_m)$. In order to satisfy the orthogonality requirement for the spatial modes, a condition for independence needs to be established.

This condition (denoted below in equation (3.2.5.2)) ensures that the spatial modes or eigenvectors are independent from one another:

$$\sum_{n=1}^{n}[\,\alpha_{in}\alpha_{jn}\,] = \delta_{ij} \qquad (3.2.5.2)$$

where δ_{ij} is the commonly used Kronecker delta function and is equal to:

$$\delta_{ij} = \begin{cases} 0, & j \neq i \\ 1, & j = i \end{cases} \qquad (3.2.5.3)$$

EOF analysis also requires that time amplitudes be uncorrelated. This is accomplished by requiring:

$$\underline{\alpha_i(t_m)\,\alpha_j(t_m)} = \beta_i\delta_{ij} \qquad (3.2.5.4)$$

Where $\beta_i=\underline{\alpha_i(t_m)}^2$ describes the variance in each orthogonal mode and the underbar denotes a time mean (Ross et al., 2014). The combination of equation (3.2.5.4) and (3.2.5.2) ensures orthogonality and possibility of analysis.

Equation (3.2.5.5) is derived from taking the covariance matrix of the echo anomaly data and multiplying by the eigenvectors and summing over number of modes, *l*:

$$\sum_{l=1}^{n}\underline{u_n\,(t_m)u_l(t_m)\alpha_{il}} = \beta_i\alpha_{in} \qquad (3.2.5.5)$$

This equation describes the *i*th mode at a given depth, *n*, or the spatial variability in each mode (Ross et al., 2014). Removing the time mean at each depth in the covariance matrix allows for the following simpler canonical form of the eigenvalue problem:

$$(\mathbf{C}-\beta\mathbf{I})\mathbf{A}=0 \qquad (3.2.5.6)$$

Where **C** is the covariance matrix (found as $C_{nl} = u_n(t_m)u_l(t_m)$ for $0 \leq l \leq n$), **I** is the identity matrix, and **A** is the eigenfunction matrix. In order for equation (3.2.5.6) to have a significant solution, the determinant of **C**-β**I** must equal zero. When this determinant is expanded, it yields a polynomial of the *n*th degree whose *n* eigenvalues follow in decreasing order from 1 to *n* ($\beta_1 > \beta_2 > ... > \beta_n$). This shows that the eigenvectors dominate the ordering of percent variance explained by a mode. The first mode representing spatial variation (β_1) contains the highest variance and each eigenvalue decreases in accordance with the variance explained. EOF analysis is beneficial because it describes the dominant physical processes using both temporal and spatial scales.

RESULTS

4.1 River Discharge

Glacial lake outburst floods (GLOFs) are occurring more frequently through Martinez Channel. Figure 4.1.1 shows river discharge data from 2003 with GLOFs indicated by the red and blue dots. Between 2003 and 2008, no GLOFs were observed. However, between 2008 and 2014, 16 GLOF events occurred, the last of which happened during the study period. Figure 4.1.2 shows isolated river discharge data collected in 2014. A GLOF (with discharge greater than 2000 m^3/s; Marín et al., 2013; Ross et al., 2015) occurred from February 1st to February 3rd of 2014 with a maximum flow of 4240 m^3/s (figure 4.1.2). A second GLOF occurred from August 18th to August 20th of 2014 with a peak flow of 3569 m^3/s (figure 4.1.2).

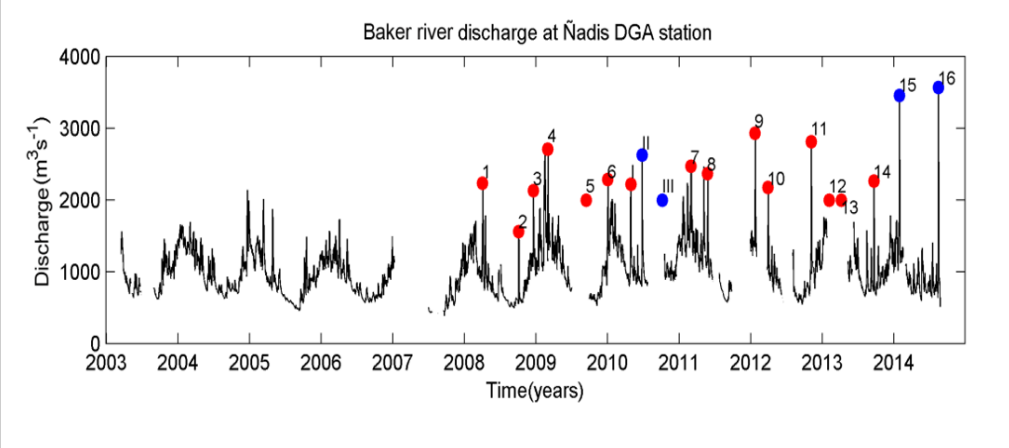

Figure 4.1.1: Discharge from Baker River collected daily at DGA station from 2003 to 2014. GLOFs are indicated by the red and blue dots where II and III represent potential GLOF events and 15 and 16 represent the GLOFs that occurred during 2014.

This study focuses on the effects of the first GLOF that occurred in February. After this event, river discharge experienced sharp increases (~305-790 m^3/s) approximately four times (April 15th, May 10th, May 28th, and July 21st of 2014). However, data collected after day 236 (August 24th of 2014) was sparse. This could be

due to machine malfunction (such as loss of battery) or elevated conditions (i.e. extreme weather) affecting the discharge readings.

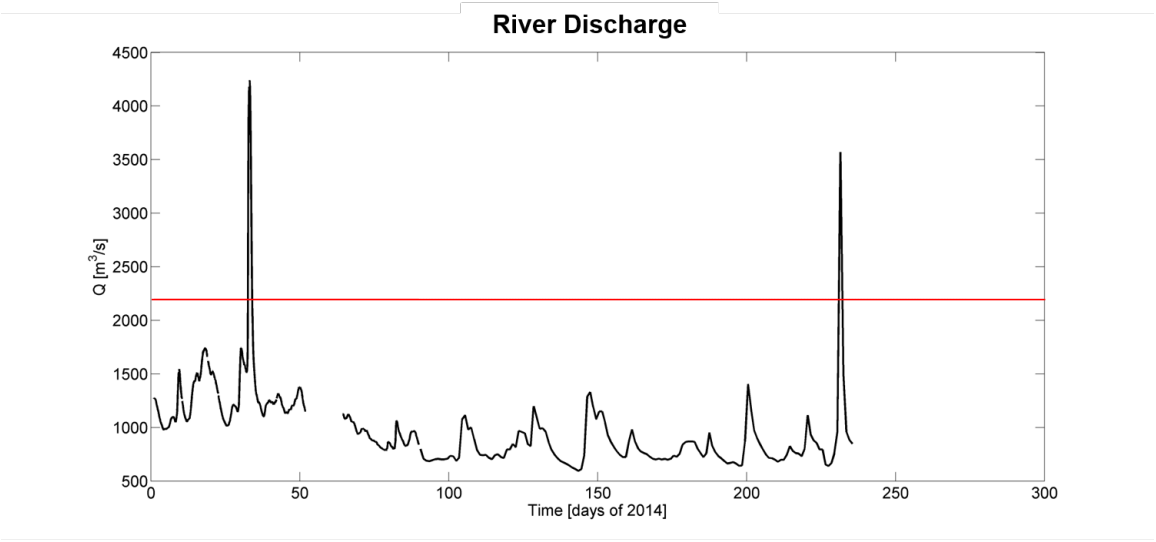

Figure 4.1.2: Discharge from Baker River collected at DGA station for the year of 2014. The red line indicates the minimum discharge required to categorize a GLOF.

4.2 Hydrographic Properties

Profiles of salinity, temperature, chlorophyll and dissolved oxygen collected from the CTD in June of 2014 (austral winter) show the most pronounced features in the upper water column (< 20 m depth; figure 4.2.1). The density, shown as sigma-t or the density minus 1000 kg/m^3 (figure 4.2.1c), and buoyancy frequency (figure 4.2.1f) show a well-defined, salinity driven pycnocline occurring at ~3-8 m depth. Surface temperatures measured around 5˚C and increased over the depth of the pycnocline (~8 m) to around 9 ˚C. Temperature reaches a maximum of 10.46 ˚C at ~44 m depth and gradually decreases to ~9.4 ˚C at 100 m depth (figure 4.2.1a). Salinity and density exhibit similar pattern to temperature in the top 50 m in that both measurements increase quickly over the depth of the pycnocline then begin a gradual increase. Surface salinity sharply decreases from ~14 g/kg to ~2.5 g/kg over 2 m then increases to 26.78 g/kg at the pycnocline (figure 4.2.1b).

Density exhibits a similar pattern with a decrease from ~11 kg/m^3 to ~2 kg/m^3 in the top 2 m then an increase to ~21 kg/m^3 at the pycnocline (figure 4.2.1c).

Chlorophyll shows elevated values (~0.2 CCI) near the surface, which decrease to zero below the pycnocline (figure 4.2.1d). Chlorophyll is a measurement of primary producers that can live in the freshwaters above the pycnocline. Meerhoff et al., (2014) found primary producers in Martinez Channel were typically located in the fresher, buoyant surface water above the pycnocline. Chlorophyll values were also highest where the water column was most oxygenated. In particular, surface dissolved oxygen levels ranged from 6.1 mL/L to 8.6 mL/L with an average value of 7.5 mL/L (figure 4.2.1e). Values decrease to ~5-5.3 mL/L around 10 m then gradually decrease throughout the water column to ~4.1 mL/L at 80 m.

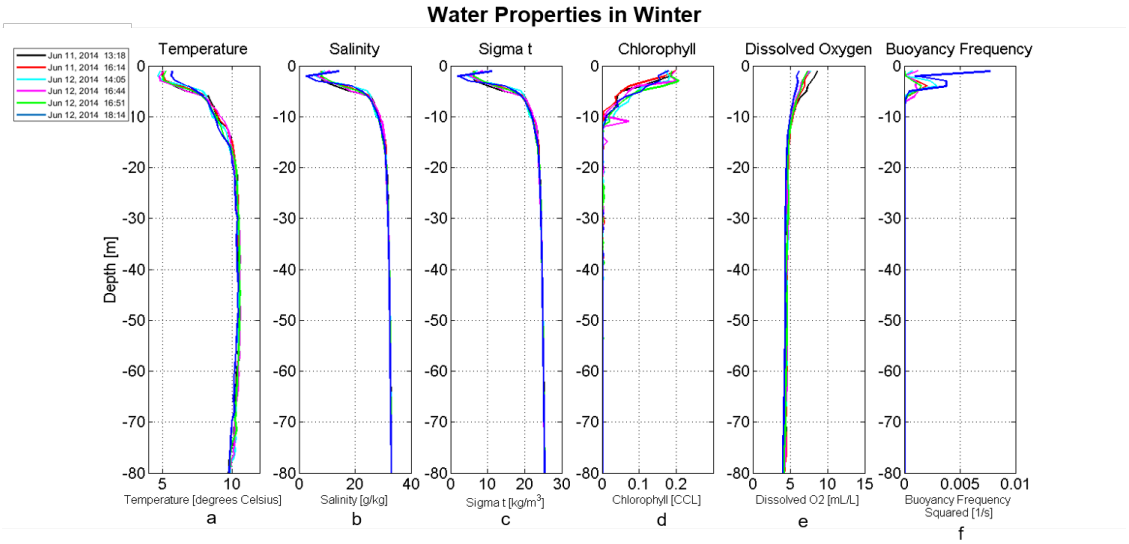

Figure 4.2.1: These subplots represent fjordic properties throughout the water column for different CTD casts in austral winter. (a) Temperature profile, (b) salinity profile, (c) density represented as sigma t, (d) chlorophyll concentration, (e) dissolved oxygen profile, (f) square of the buoyancy frequency showing stratification.

Similar to the water property profiles collected during the austral winter months, profiles from austral summer (November, December, and January) also exhibit strong salinity

driven stratification in the upper water column (< 20 m depth; figure 4.2.2). In particular, the surface layer (0 to ~8 m depth) contains freshwater (0 g/kg salinity) with a sharp increase to ~28 g/kg thereafter, where it remains constant in the remainder of the water column (figure 4.2.2b). Elevated surface temperatures of ~10-11 ˚C were found in the top 10 m of the water column (figure 4.2.2a), as expected during the austral summer months. December temperatures achieve a minimum of 7 ˚C at ~10 m then warm until they reach 8.5 ˚C at 16 m depth. November temperatures decrease sharply to a minimum of ~8.3 ˚C at ~13 m depth then increase to 8 ˚C around 16 m depth similar to December's pattern. To the contrary, January temperature decreases to ~9.5 ˚C at 8.5 m depth then increases to return to its surface temperature of ~11 ˚C. Below this it continues reducing until 8.5 ˚C at 16 m depth. Overall, the temperature profiles indicate a three-layer structure, with warmer waters at the surface and at depth and a cooler layer just below the pycnocline, which can lead to double diffusive mixing in this fjord system (Perez-Santos et al., 2014). Density does not follow the three-layer structure present in the temperature but rather the sharp increase at the pycnocline (~8 m) then the gradual increase similar to that of the salinity profile (figure 4.2.2b and figure 4.2.2c). Elevated values of buoyancy frequency occur at ~8 m depth with an average value of 0.003 s^{-2} (figure 4.2.2f). This supports the pycnocline location at 8 m depth and the approximated location is illustrated by the orange line drawn in figure 4.2.2.

Chlorophyll data is more active during summer than in winter but follows the same pattern of decreasing to zero just below the pycnocline (~8 m) (figure 4.2.2d). Measurements taken in November and December show surface values of 0.1 CCI where

January exhibits surface chlorophyll levels of 0.2 CCI (figure 4.2.2.d). This aligns with results from austral winter showing primary producers in freshwater and not in the deeper saline layer.

Surface dissolved oxygen levels for November and December were recorded as 8 mL/L and 6.5 mL/L, respectively. These values were relatively constant from the surface to the pycnocline and experienced a sharp decrease of about 1.5 mL/L in the 3 m below the pycnocline (figure 4.2.2e). Values then decrease gradually to 4.44 mL/L and 3.48 mL/L in November and December, respectively. Dissolved oxygen in January shows a steep increase from 9.4 mL/L to 12.8 mL/L in the first 6 m of the water column then a steep decrease to ~9.4 mL/L over the next 4 m. It then gradually decreases similar to the other summer months where it is 6.4 mL/L at 80 m depth.

Dissolved oxygen concentrations can be affected by wind influencing interactions between air and surface waters. Some studies have shown that wind can also induce mixing (Ross et al., 2015). Wind influence is an important parameter in understanding fjord physics and thus was considered in this study.

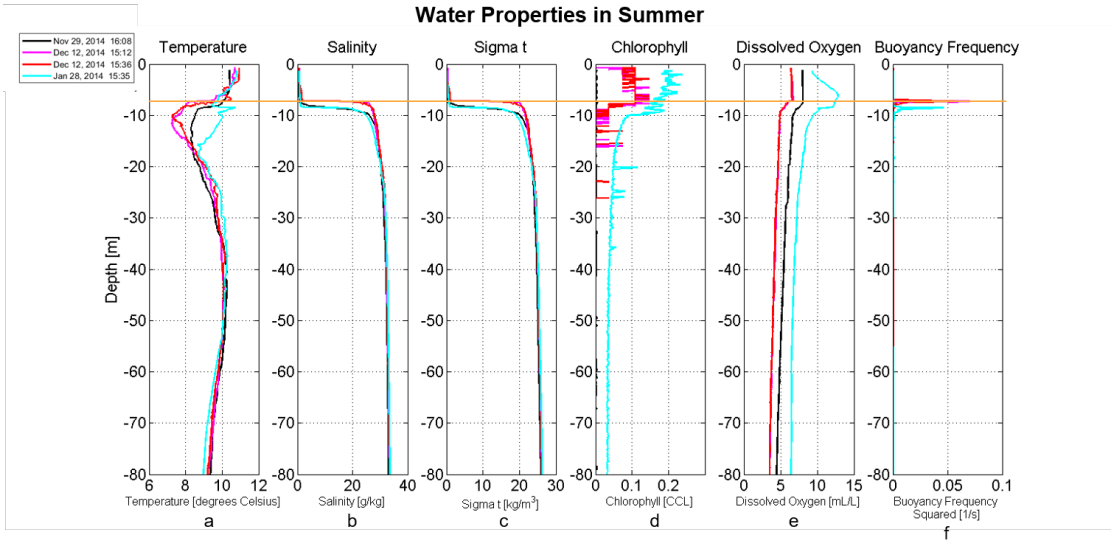

Figure 4.2.2: These subplots represent fjordic properties throughout the water column for different CTD casts in austral summer. The orange line is an estimate of the pycnocline location. (a) Temperature profile, (b) salinity profile, (c) density represented as sigma t, (d) chlorophyll concentration, (e) dissolved oxygen profile, (f) square of the buoyancy frequency showing stratification.

4.3 Wind Data

A lowpass filter of the wind removing trends less than 5 days begins in the south-eastward direction for the first 40 days of 2014 (January 1st to February 9th). From approximately day 40 to day 90 (February 9th to March 31st), the direction is north-east. On approximately day 100 (April 10th), the wind remains primarily eastward for the remainder of 2014 but fluctuates between north and south with a strong southern pulse (~4 m/s) at day 150 (May 30th). Around day 270 (September 27th), the wind becomes north-eastward.

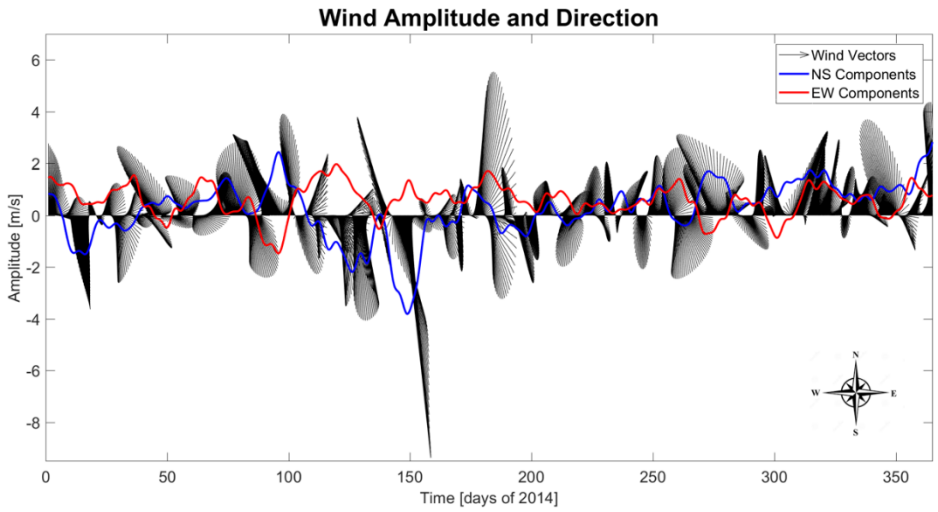

Figure 4.3.1: Wind amplitude and direction through 2014 recorded from the Chilean Navy Lighthouse seen in figure 3.1. Regarding the components, positive values represent directions north and east and negative values represent south and west. The vectors follow the compass directions indicated by the compass rose in the bottom right.

4.4 Current Velocity

Velocity data was sparse for the first 40 m of the water column. This is likely due to an insufficient amount of particle activity (or scatterers) used by the ADCP to derive velocity data from backscatter. Subsequent data analysis required complete data so gaps were filled with the average velocity at their corresponding depth. The raw along-channel velocity and the 'filled' along-channel velocity with respect to time (*x*-axis) and depth (*y*-axis) are shown in figure 4.4.1a and figure 4.4.1b, respectively. Harmonic analysis prediction and interpolation were both considered in filling the data. However, these methods produced values that did not appear consistent with the surrounding velocity values, indicating a false representation of velocity patterns. It was noted throughout the analysis process that filling missing data with average values might still cause a misrepresentation of results although it was the better option of the three explored methods. The same method was used for the across-channel velocity (not shown).

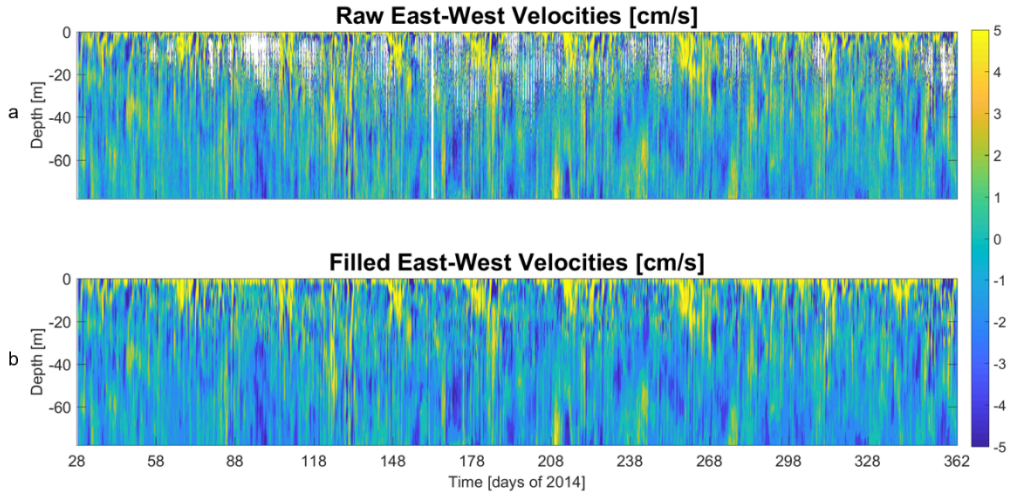

Figure 4.4.1: (a) Along-channel (east-west) velocities as measured from the ADCP, (b) along-channel velocities with gaps filled by average velocity values at the corresponding depth. Positive values represent an eastward flow whereas negative values indicate westward flow

Elevated surface velocities between ~60 and 70 cm/s occur every ~20-30 days in a north-eastern direction as seen in figure 4.4.2. These findings are consistent with the baroclinic annular mode (BAM) producing a subtropical cyclone every ~20-30 days, as studied in Ross et al., (2015). This is further elaborated upon in Section 5.

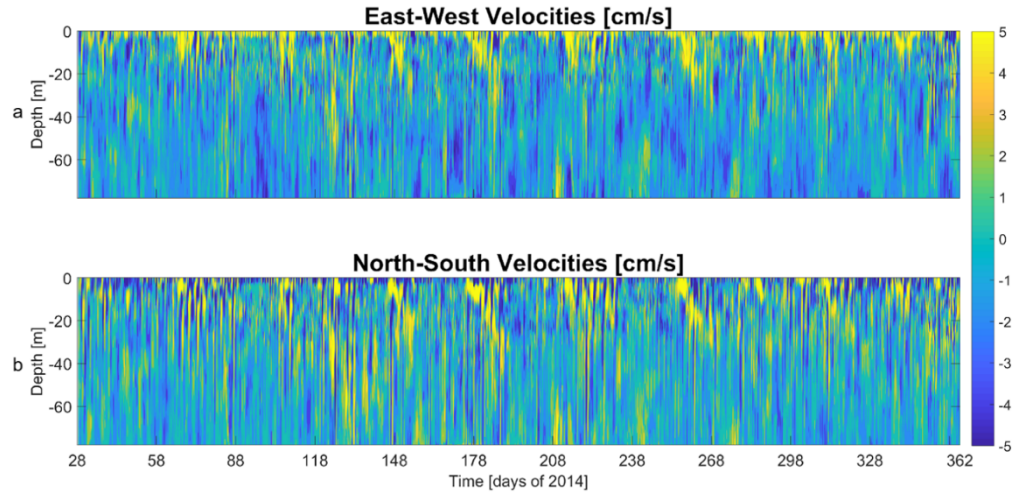

Figure 4.4.2: (a) Along-channel velocities filled using the method described in section 4.4 (b) across-channel velocities filled using the same method. Positive values indicate eastern and northern directions and negative values represent western and southern directions.

Velocities during the GLOF (day 32 to 34; February 1st to February 3rd) don't exhibit marked variation compared to the rest of the year. However, figure 4.4.3 shows

significant eastward surface flow during the GLOF, which represents flow into the channel. Surface velocities are strongest in the North-East direction for the first third of the GLOF and South-East direction for the remainder of the GLOF.

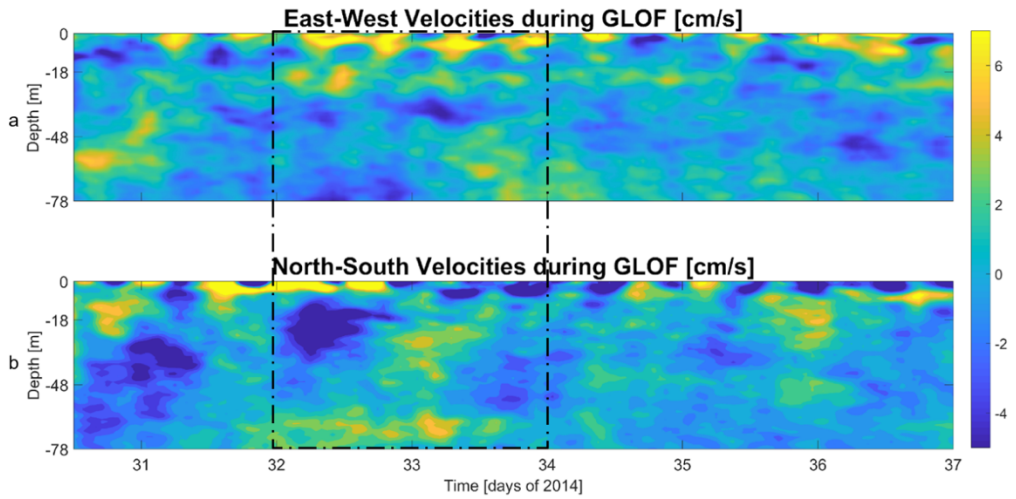

Figure 4.4.3: (a) Along-channel velocities surrounding the GLOF event and (b) across-channel velocities surrounding the GLOF event with the black box indicating the time frame in which the GLOF occurred. Positive values indicate eastern and northern directions and negative values represent western and southern directions.

Next, the echo anomaly was evaluated to explore pycnocline vertical motions and biological activity throughout the water column over time. The goal is to determine how modulations of the pycnocline relate to current velocities and water column properties of the fjord, and how biology (zooplankton) responds to the fjord physics.

4.5 Echo Anomaly

Echo anomaly results show elevated signal (>1.5 dB) in the upper ~50 m of the water column from day 28 (January 28th) to day 47 (February 16th) as seen in figure 4.5.1. The GLOF occurs during this time period from day 32 to 34 (February 1st to February 3rd) and features elevated activity in the water column. Echo anomaly in the top 2 m shows a low signal (~ -4.3 dB) occurring simultaneously to the elevated signal that appears in the first ~50 m of the water column. The low echo anomaly signal in the first 2 m during this time might be due to the ADCP not being able to penetrate through the thick layer of scatterers

(suspended sediments from the glacial water, often called glacial flour) that accumulates near the pycnocline due to the GLOF (Marin et al., 2013).

In addition to the elevated echo anomaly signal that is seen during the GLOF, elevated values also appear near the pycnocline depth (~8-10 m) every ~20-30 days (figure 4.5.1). The strongest signal (~2.7 dB) is at ~3.5 m depth around day 108. This pattern was found in Ross et al., (2015) to be depressions of the pycnocline due to a weather phenomenon in the southern hemisphere known as the baroclinic annular mode (BAM). The BAM can be described as a proxy for the 'storminess' of the southern hemisphere, with low pressure systems impacting the region every ~20-30 days. It is characterized by eddy fluxes of heat shedding off of the equator (Marshall et al., 2017; Thompson and Barnes, 2014). These eddy fluxes manifest as storms with high wind and precipitation moving from west to east in the southern hemisphere. However, the data set used in Ross et al., (2015) only encompassed three months of the year (austral summer and fall) whereas this study encompasses a full year. The full year of data used in this study suggests that the BAM produces a deepening of the mixed layer (pycnocline) throughout 2014 as was seen for the three months of data in 2010 evaluated in Ross et al., (2015). This will be considered further in Section 5.

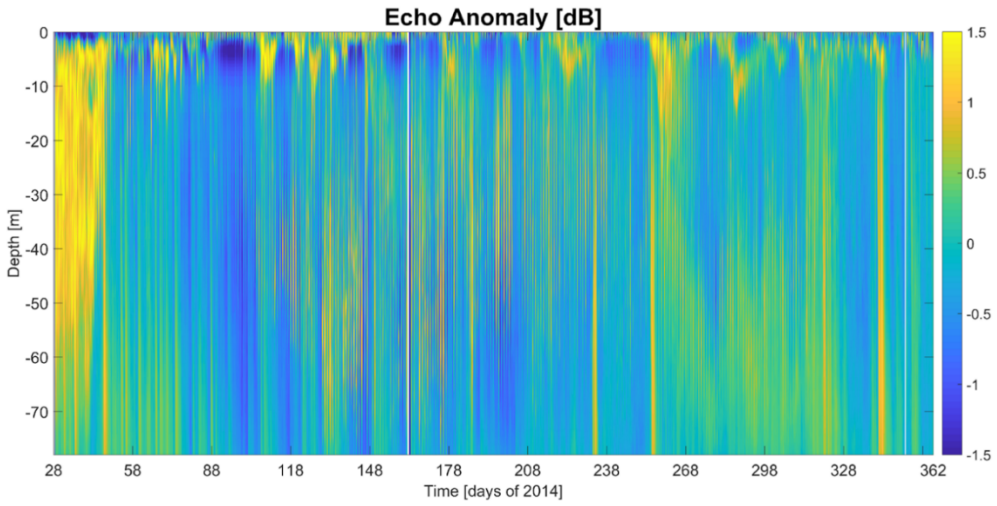

Figure 4.5.1: Echo Anomaly as calculated from the backscatter using the method described in section 3.2.2. This is intended to give an idea of activity in the water column as it is a measure of particle feedback.

A distinct vertical pattern appears in the echo anomaly during austral autumn on day 90 (March 31st) that persists through day 320 (November 16th of 2014) (figure 4.5.2a-d). This pattern occurs at a diurnal periodicity (~24 h) and therefore is not driven by the semidiurnal tide (period of 12.42 h) and is therefore indicative of diel vertical migration (DVM) of zooplankton. The dominant frequencies found in the echo anomaly and the presence of zooplankton in the fjord will be investigated further in the discussion (Section 5). The vertical pattern is most prevalent between ~20-40 m depth during the winter season (day 195 to 200; July 14th to July 19th ; figure 4.5.2b) and persists throughout winter to the spring. In spring, the pattern attenuates but a strong signal remains between 40 and 70 m depth. The pattern appears to end around day 320 (November 16th; austral spring; figure 4.5.2c) for the remaining 33 days of 2014, indicating that DVM pattern is not present.

In order to determine the dominant modes of variability in the fjord throughout the year of 2014, an empirical orthogonal function (EOF) analysis will be carried out on the echo anomaly data. This analysis will shed light on the spatial and temporal variability of the

echo anomaly and determine how much of the variance in the system is explained by the diurnal pulses that are thought to be due to DVM of zooplankton.

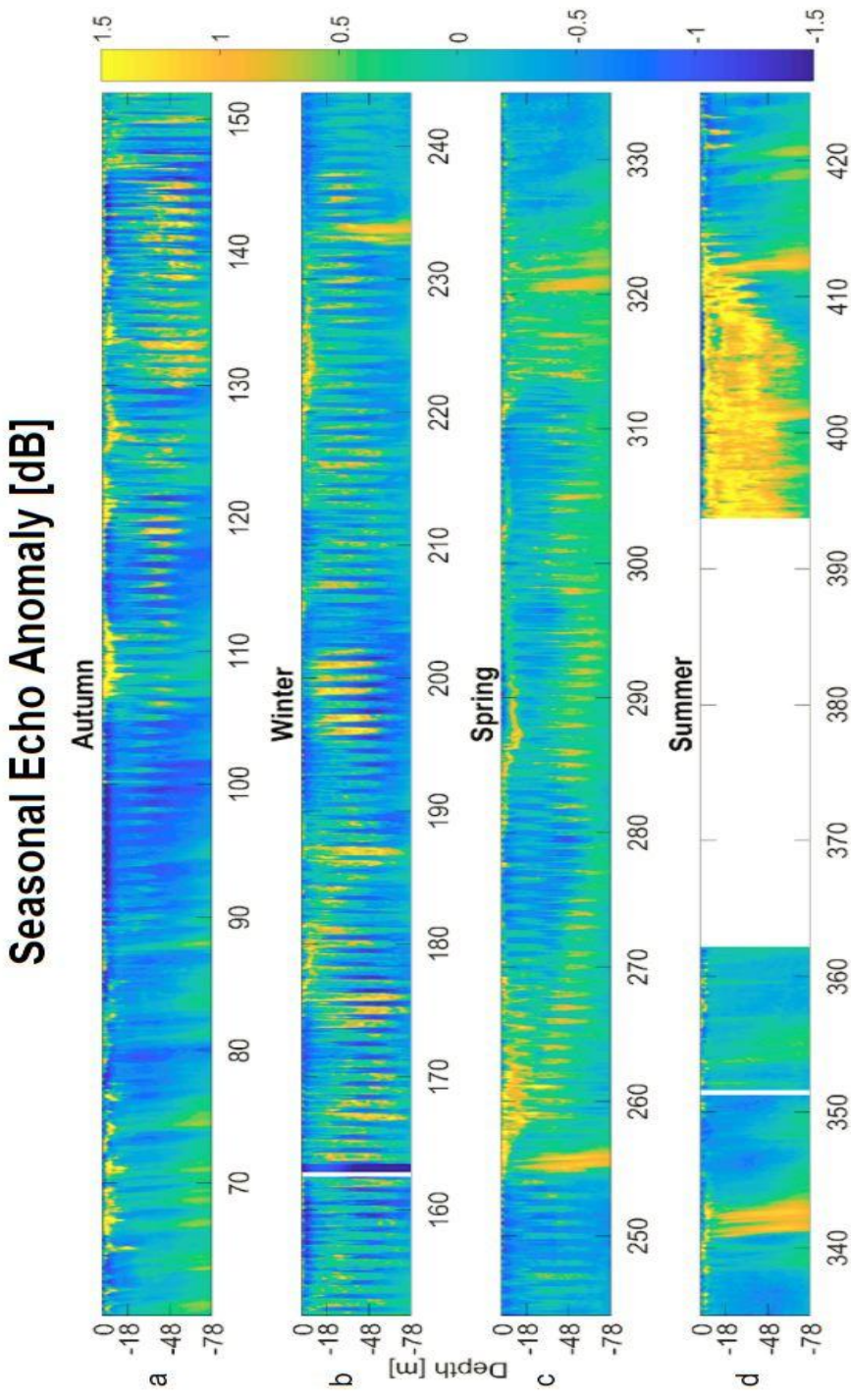

Figure 4.5.2: Echo anomaly for the (a) autumn, (b) winter, (c) spring, and (d) summer austral seasons of 2014.

4.6 EOF Results

To further investigate activity in the water column, an empirical orthogonal function (EOF) analysis was conducted. The results explain the dominant spatial (depth varying) and temporal (time varying) behavior in a data set by breaking it up into orthogonal modes that explain variance within the fjord. The variance can be simply described as deviations from the mean. The dominant spatially varying mode (EOF eigenfunction) in the echo anomaly (figure 4.5.1) displays a unidirectional signal for Mode 1 (M1 explains 56.2% of the variance), a two-layered signal for M2 (explaining 14.9% of the variance), and a three-layered signal for M3 (explains 10.4% of the variance) (figure 4.6.1). The total variance explained by Modes 1 to 3 is 81.5%. The amplitude of M1 is negative throughout the majority of the water column. A minimum amplitude of -0.13 dB is reached at ~40 m. This negative signal indicates that M1 includes deviations of the echo anomaly signal that are below the mean. This could be due to the DVM of zooplankton being absent during the daytime, which produces 'lower' values of the echo anomaly. M2 displays a maximum of 0.14 at 7 m. It remains positive until ~40 m depth where it then becomes negative. The positive values indicate that M2 displays above average signal in the upper portion of the water column (< 40 m depth) and below average signal at depth (figure 4.6.1). As the pycnocline is located in the upper water column, M2 is a product of pycnocline motions (at the tidal and BAM periodicity) dominating the upper water column.

The three-layered signal associated with M3 depicts a negative signal near the surface (from ~0 to 18 m depth) followed by a positive signal (between ~18 and 50 m depth) and

a negative signal at depth (figure 4.6.1). The three-layer structure of the third mode indicates that the signal is above average mid water column and is below average near the surface and near the bottom. The spatially varying structure of Mode 3 could be indicative of primary zooplankton congregation depths during different austral seasons. In order to determine the dominant frequencies present in the temporal variability of the first three EOF Modes, a spectral analysis will now be done on the temporally varying (principal components or eigenvalues) of each EOF mode of the echo anomaly.

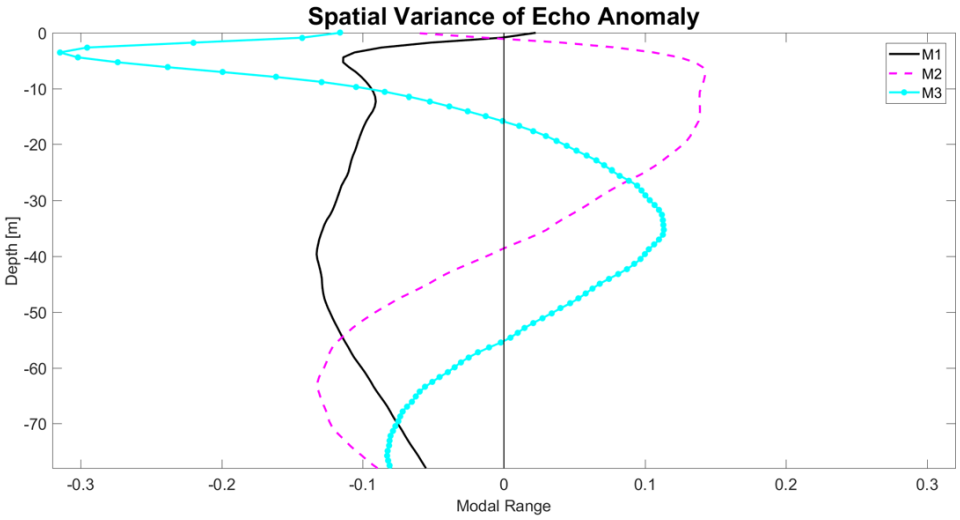

Figure 4.6.1: Spatial variation of the echo anomaly generated through EOF analysis described in section 3.2.5. This shows deviations from the mean echo anomaly signal. Mode 1 explains the most variance in the fjord (56.2%) and is indicated by the unidirectional negative signal in black. Mode 2 (in pink) explains 14.9% and shows a two-layered signal. Mode 3 (light blue) explains 10.4% and exhibits a three-layered structure.

4.7 Spectra Results

A spectral analysis was applied to the principal components of each orthogonal mode of the echo anomaly (figure 4.7.1). Mode 1 exhibits highest energy at low frequencies and at 1 cpd. A 95% confidence interval (red line in figure 4.7.1) was used to determine if the periodicity can be considered significant, where a peak in the spectra larger than the red line indicates statistical significance. Mode 2 shows a similar pulse at 1 cpd but contains less energy than Mode 1 at 1 cpd. It is around 89 dB^2/cpd^2 whereas Mode 1 is 161

dB^2/cpd^2. Mode 3 does not show significant energy at frequencies greater than 0.01cpd (~96 days), indicating that it likely explains seasonal variability in water column scatterers, or zooplankton.

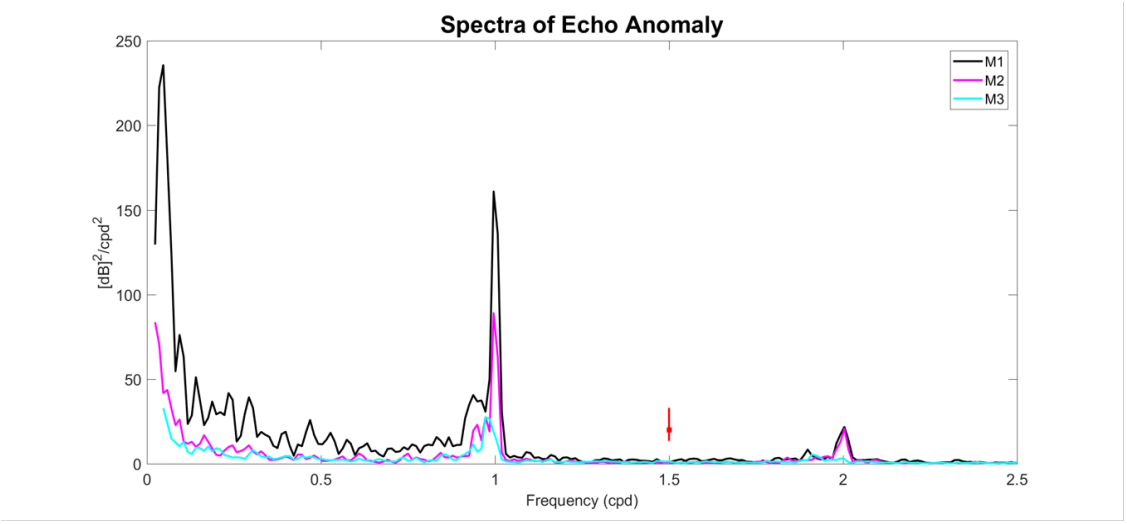

Figure 4.7.1: Spectral analysis of dominant modes found in the echo anomaly by the eof analysis described in section 4.5. The red bar represents a 95% confidence interval. Mode 1 (black) explains the most variance in the fjord (56.2%), Mode 2 (pink) explains the second most (14.9%) and Mode 3 (light blue) explains the third most (10.4%).

In order to compare the dominant frequencies found in the spectra of the echo anomaly EOF modes to the those found in the echo anomaly itself, a spectral analysis was applied to each depth of the echo anomaly (figure 4.7.2). For the spectra on the echo anomaly, high energy was found at low frequencies (<0.5 cpd) throughout the water column, and especially in the upper 10 m of the water column (figure 4.7.2). This is likely attributed to synoptic variability (wind patterns) forced by the BAM, GLOF events increasing suspended sediments in the fjord or seasonal variations in biological abundance (zooplankton) in the fjord. In addition, high energy (~1.4 dB^2/cpd^2) is observed at 1 cpd between 8 and 75 m depth. Also, as expected due to the semi-diurnal tide being dominant in this fjord, there is elevated energy at 2 cpd between 3.5 and 60 m depth. However, these results show that there is greater energy occurring at 1 cpd mid water column, indicating that the semi-diurnal tide does not bear the greatest effect on the variance of

the fjord, and rather, diurnal variations dominate. The diurnal signal is attributed to zooplankton DVM patterns. However, the echo anomaly can feature elevated signals for scatterers in the water column that are not of biological origin. To filter out the signal due solely to zooplankton, the volume backscatter, *Sv*, will now be considered.

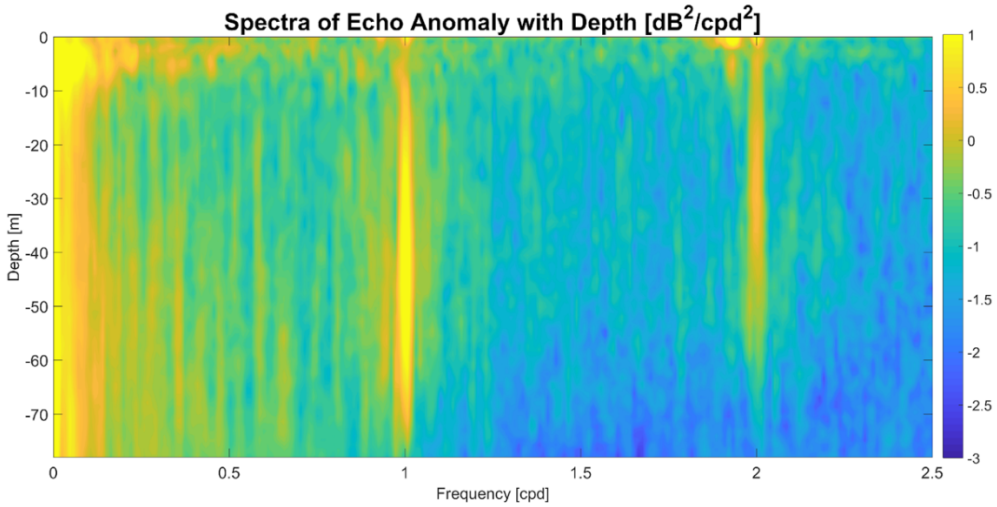

Figure 4.7.2: Spectral analysis of the echo anomaly as described in section 3.2.4 conducted over the full time series at each depth.

4.8 Volume Backscattering Strength (Sv)

Since the diel vertical migration of zooplankton occurs once per day, the volume backscatter (*Sv*) was used to investigate DVM patterns found in Martinez Channel, as the EOF and spectral analyses indicated that the dominant mode of echo anomaly variability could be due to this pattern. Similar to the echo anomaly (figure 4.5.1) an elevated *Sv* signal (~> -17 dB re 1 m^{-1}) is apparent at the pycnocline (figure 4.8.1), with the most pronounced signal from day 106 to 112 (April 16th-22nd; austral Autumn). This is because although particles with smaller diameters are removed, the *Sv* signal still registers the density interface because it represents a plane of different density (large particles >5 mm in diameter) instead of individual particles.

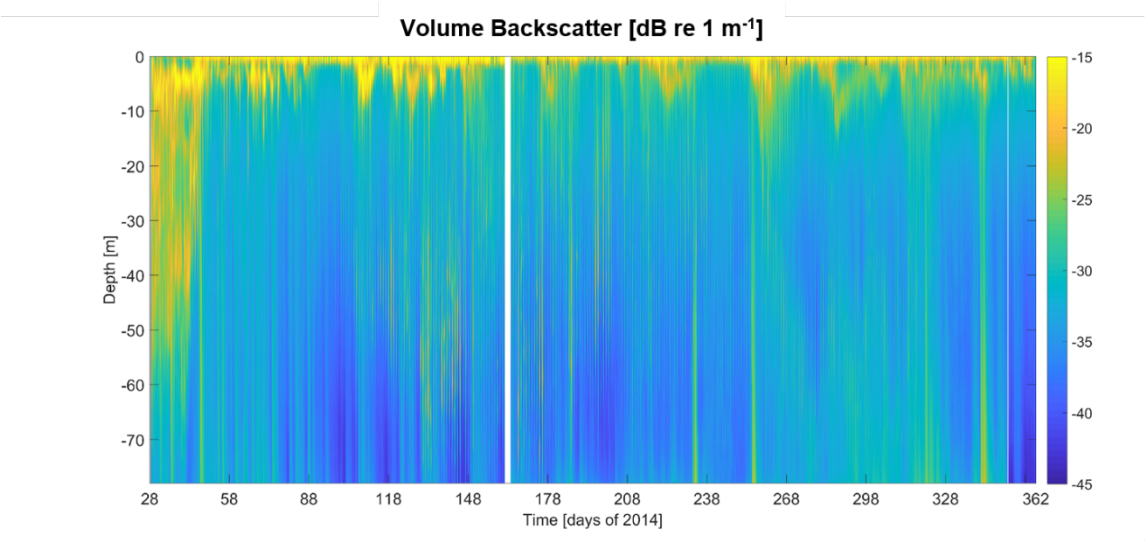

Figure 4.8.1: Volume Backscatter intended to give an idea of zooplankton activity in the water column. Calculated using the method described in section 3.2.3.

In addition to the elevated *Sv* signal at the pycnocline, vertical patterns are also prominent throughout the time series due to diel vertical migration of zooplankton. The pattern begins at approximately day 90, similar to that of the echo anomaly and ends on approximately day 320 (figure 4.5.2; figure 4.8.2). During the GLOF, there is an elevated signal (~> -17 dB re 1 m^{-1}) between days 28 and 50 from 5-10 m depth with a less intense, yet still elevated, signal between 10-50 m depth (~> -22 dB re 1 m^{-1}) becoming negligible below 30 m depth (figure 4.8.2). This could be due to an increase in biological activity or larger sediment 'flocs' (aggregations of sediment) brought in with the GLOF floodwaters settling in the water column. This is addressed in greater detail in Section 5. Next, a representative week from each austral season will be analyzed to investigate seasonal variation in volume backscatter (figure 4.8.2).

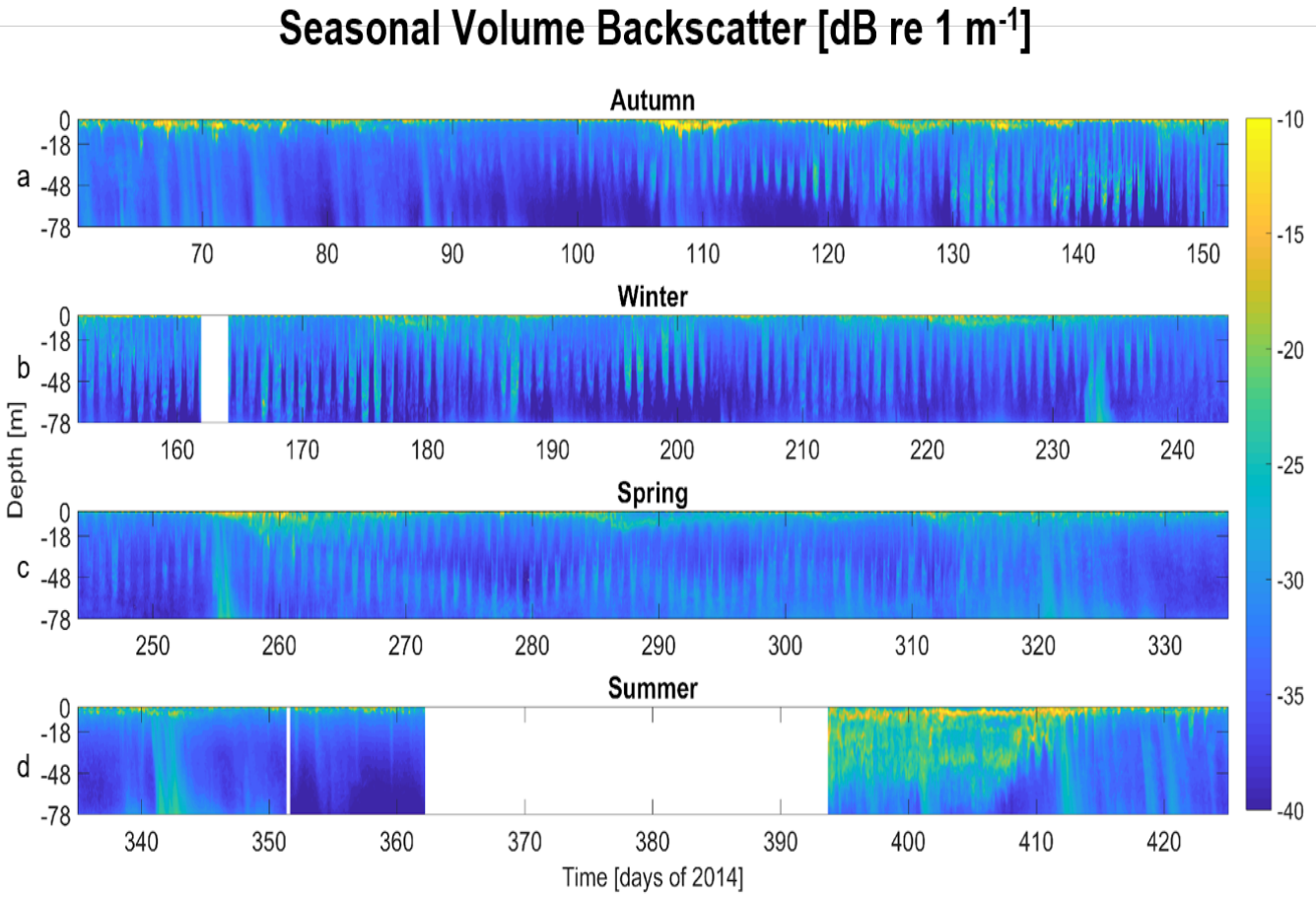

Figure 4.8.2: Volume backscatter for the (a) autumn, (b) winter, (c) spring, and (d) summer austral seasons of 2014.

4.9 Seasonal Patterns in Volume Backscatter (Sv)

To investigate seasonal variation in *Sv*, one week from each austral season was chosen qualitatively based on when the most prominent vertical pattern appeared.

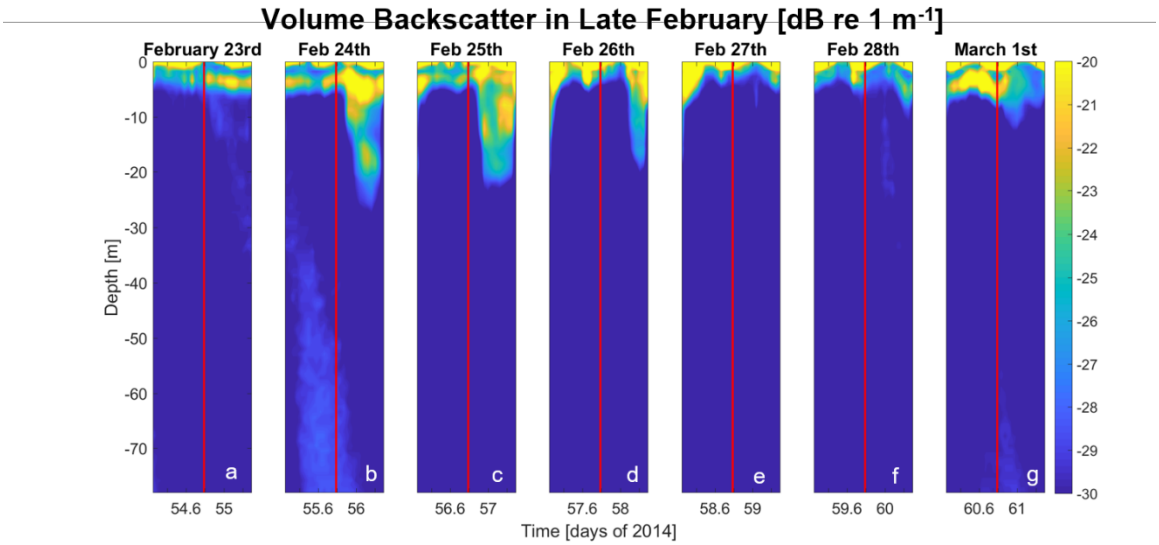

Figure 4.9.1: Representative week of volume backscatter recorded near the end of February with sunset times denoted by vertical red lines and sunrise times separating the subplots a-g. In DVM, it would be expected to see a higher volume backscatter signal after sunset and before the following sunrise. There is slight night-time activity below the pycnocline in subplots b, c, and d, which could be attributed to DVM.

For figure 4.9.1- figure 4.9.4, each day is represented by a subplot with the red line indicating the time of sunset. The week of February 23rd to March 1st (austral summer) showed consistently elevated *Sv* signal near the surface (> -4 m; ~ 20 dB re 1 m^{-1}; figure 4.9.1). February 23rd showed an elevated signal (-19.5 dB re 1 m^{-1}) around -3.5 m. Below this, a slightly elevated signal (~ -28 dB re 1 m^{-1}) was seen in a pattern descending the water column with time, stopping after sunset on February 24th. This is attributed to zooplankton congregating at the pycnocline and subsequently descending before sunrise. The night of February 24th showed the highest *Sv* signal for the week near the surface (~ -17 dB re 1 m^{-1}), which remained coherent up to ~25 m depth. After sunset on February 25th, a similar pattern as the previous night emerged with a high signal (~ -18 dB re1 m^{-1})

at 3.5 m continuing until ~23 m depth. The night of February 26th showed a less pronounced signal with a similar pattern extending ~20 m depth. Overall, average activity between the pycnocline and ~78 m during the daylight hours was slightly less than between sunset and sunrise for this week (-31.54 compared to -31.19 dB re 1 m^{-1}), alluding to faint, but present, DVM patterns.

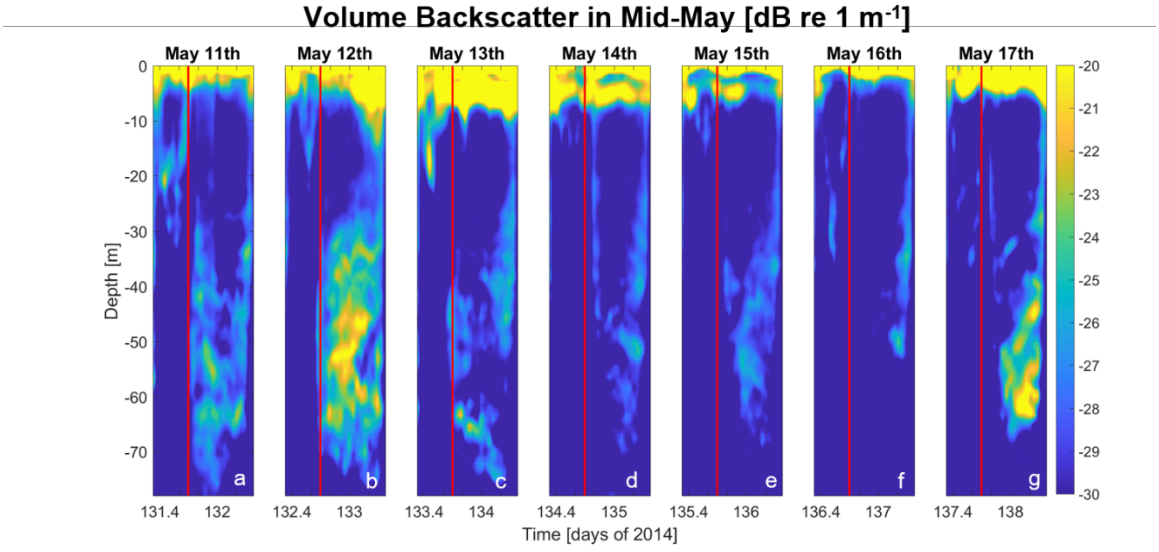

Figure 4.9.2: Volume backscatter plotted for a week in mid-May with sunset times denoted by vertical red lines and sunrise times separating the subplots a-g. An elevated signal (< - 28 dB re 1 m^{-1}) is present between sunrise and sunset each day which is indicative of DVM. The signal is particularly high the night of May 12th (subplot b).

The week of May 11th, 2014 (austral autumn) showed a more distinct pattern of elevated signals occurring after sunset (figure 4.9.2). Between 30-70 m depth, signals > -28 dB re 1 m^{-1} appeared after sunset and ended before sunrise for each day, with the most prominent signal occurring the night of May 12th (~ -20 dB re 1 m^{-1}). There was also an elevated signal (~ -12 dB re 1 m^{-1}) near the pycnocline (>-5 m) during this day which continued roughly through the early morning of May 15th where it subsided until another pulse (~ -19 dB re 1 m^{-1}) after sunset. May 17th showed elevated *Sv* above the pycnocline (~ -14 dB re 1 m^{-1}) during the day and continuing through the night. Overall, there was a greater average feedback during the night (-29.14 dB re 1 m^{-1}) than during the day

(-31.98 dB re 1 m^{-1}). This reinforces the hypothesis of DVM occurring in Martinez Channel and implies that these patterns are more pronounced during austral autumn and winter months than austral spring and summer. This is consistent with Valle-Levinson et al., (2014) that found a more distinct DVM pattern in winter than in spring.

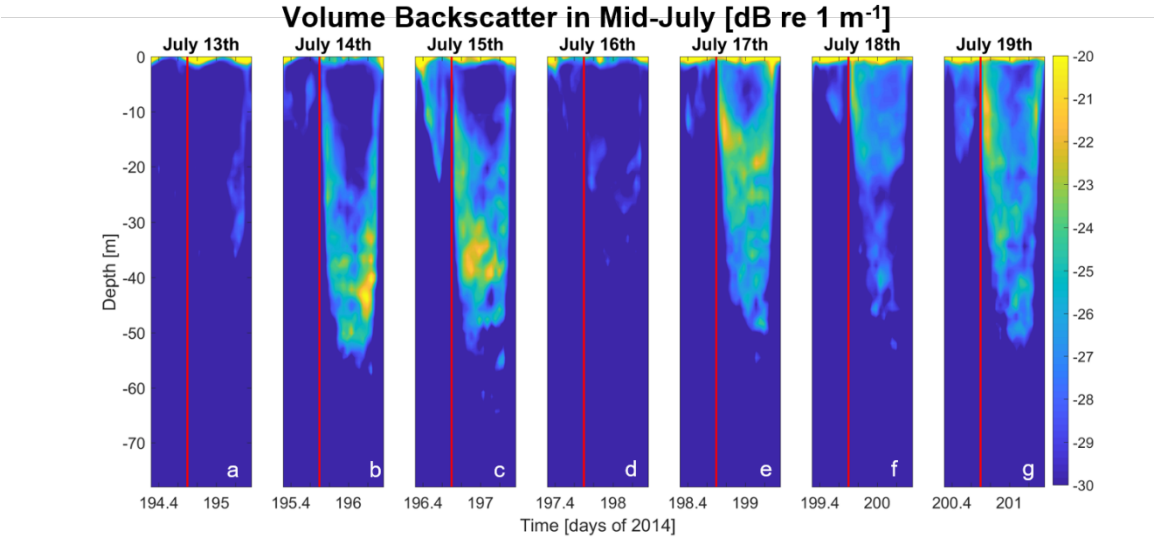

Figure 4.9.3: Volume backscatter plotted for a week in mid-July with sunset times denoted by vertical red lines and sunrise times separating the subplots a-g. An elevated signal (< -28 dB re 1 m^{-1}) is present between sunrise and sunset each day, with prominent signals occurring July 14th, 15th, 17th, 18th, and 19th (subplots b, c, e, f, and g) which is indicative of DVM.

Among each of the arbitrary weeks chosen to investigate a DVM pattern, the week of July 13th (austral winter) showed the most distinct DVM pattern (figure 4.9.3). An elevated signal (> -28 dB re 1 m^{-1}) was most prevalent during the nights of July 14th, 15th, 17th, 18th, and 19th. There was limited activity near the pycnocline during this week, but signals remained strong near the surface (~ -16 dB re 1 m^{-1} in the top 2 m of the water column). The zooplankton were more active during the night, with an average volume backscatter feedback of -32.13 dB re 1 m^{-1} compared to -35.94 dB re 1 m^{-1} feedback during the weekdays. The patterns show the zooplankton migrating up to the surface at dusk, descending down to ~20-60 m during the night, and then migrating up to the surface at dawn before descending to deep depths (<80 m) during the day. This is

consistent with twilight vertical migrations of zooplankton found in Reloncavi Fjord, Chilean Patagonia (Valle-Levinson et al., 2014). This will be further investigated in the discussion (Section 5).

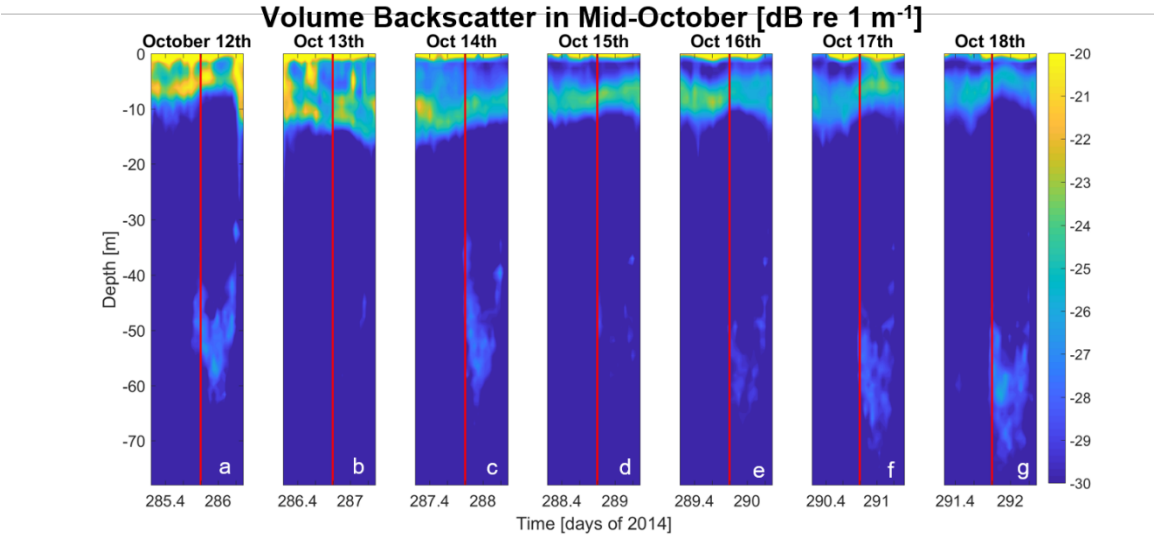

Figure 4.9.4: Volume backscatter plotted for a week in mid-October during a period of pycnocline depression with sunset times denoted by vertical red lines and sunrise times separating the subplots a-g. Elevated signals (< -28 dB re 1 m^{-1}) are present October 12th, 14th, 16th, 17th, and 18th (subplots a, c, e, f, and g), indicating that DVM pattern could still be present during periods of pycnocline depression.

The week of October 12th (austral spring) was investigated as it occurs during a period of hypothesized pycnocline depression resulting from the BAM. This is evident from the attenuating signal around the pycnocline after October 12th that also extends deeper into the water column (~12-15 m). It is important to investigate the behavior of zooplankton during this recurring trend within Martinez Channel to better understand how fjord biology reacts to an observed pattern. During this week, there was a consistent signal >-28 dB re 1 m^{-1} above ~13 m, indicative of pycnocline depression (figure 4.9.4). Elevated signal indicating DVM pattern was present but remained between ~ -28 and -25 dB re 1 m^{-1} during night hours and at depths below 30 m. It was especially prevalent during the nights of October 12th, 14th, 16th, 17th, and 18th between ~30-70 m depth. This indicates that zooplankton migration can still occur during periods of pycnocline

depression, however the zooplankton do not migrate the full depth of the water column. This could be due to the mixture of fresh and salt water at the pycnocline interface creating unfavorable conditions for the zooplankton, or the storm-induced turbulent motion near the surface inhibiting their migration.

Now, the discussion will investigate the role of wind forcing on pycnocline depressions in Martinez Channel and subsequent impacts on biology. The discussion will also investigate how the GLOF changed existing conditions within the fjord regarding physics and biology.

DISCUSSION

The overarching goal of this study is to determine how the physical and biological properties of a glacial fjord vary throughout a year. To accomplish this goal, the following two research questions were established: 1) How do the hydrodynamics and water column properties of the fjord vary intra-annually and in the presence of a GLOF? And 2) How do these intra-annual variations link to the biology of the fjord? In order to elaborate on these goals, the following section connects the physical patterns found in this study to the biological patterns and elaborates on how each of these are affected by a glacial lake outburst flood. Particularly, the influence of the BAM on fjord circulation and DVM is discussed as well as how the GLOF interacts with fjord biology and the wind-forcing from the BAM.

5.1 Fjord Physics

Subtidal or residual circulation within a fjord is typically density driven (gravitational circulation; Farmer and Freeland 1983). This long-term circulation is forced by density differences in the freshwater surface layer and underlying saltwater layer. The freshwater layer, derived mostly from river water, typically flows out-fjord at high velocities over the top of a sluggishly inflowing saltwater layer, incorporating some saltwater into its flow. The underlying saltwater layer also pulls some freshwater with it as it flows in-fjord. This induces mixing at the density interface (pycnocline; figure 5.1.1).

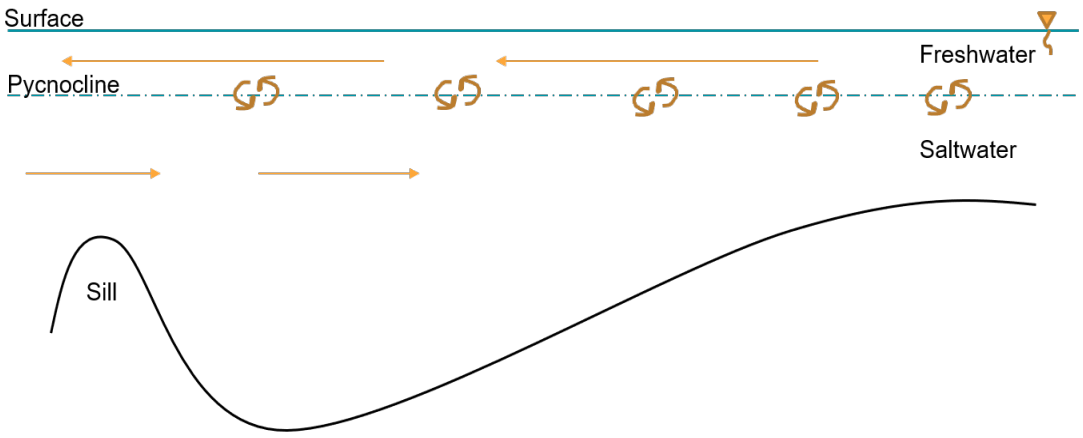

Figure 5.1.1: Gravitational Circulation, typical in fjords and estuaries. The orange arrows denote relative flow velocity and the brown arrows are indicative of mixing along the pycnocline. The water surface is indicated by the inverted triangle on the right.

A vertical profile of gravitational circulation would show net outflow above the pycnocline with inflow through the rest of the water column (figure 5.1.2). In Martinez Channel, average along-channel velocities were used to depict the subtidal flow pattern throughout the measurement period.

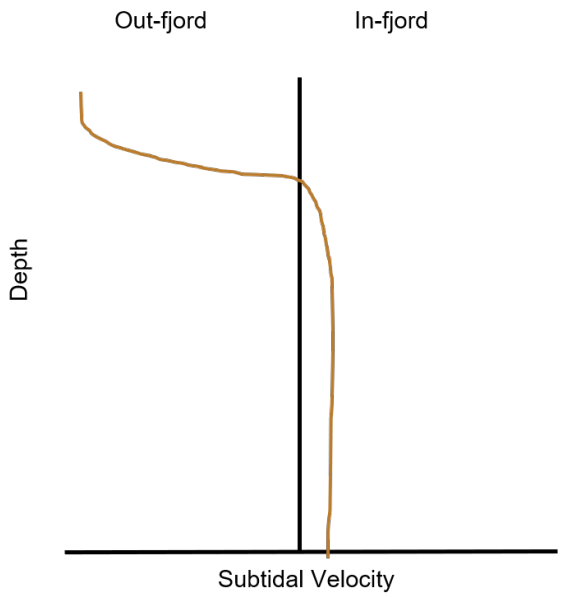

Figure 5.1.2: A vertical flow profile of gravitational circulation. River discharge contributes to a relatively fast net out-fjord flow above the pycnocline (where velocity changes direction). A sluggish inflow is provided by the underlying salt water to balance inflow and outflow.

Instead of displaying a flow profile indicative of gravitational circulation, Martinez Channel exhibited flow directed eastward (in-fjord) above ~35 m depth with an underlying outward flow (figure 5.1.3). This result is surprising, especially in light of the westward river flow from Baker River. This suggests that density differences might not be the primary driver of circulation in Martinez Channel throughout the year. Valle-Levinson et al. (2014) suggested that wind forcing, density gradients external to the fjord, and tidal forcing can influence fjord circulation. Since wind data was available for 2014, it was investigated as one of the potential influences on the subtidal flow in Martinez Channel.

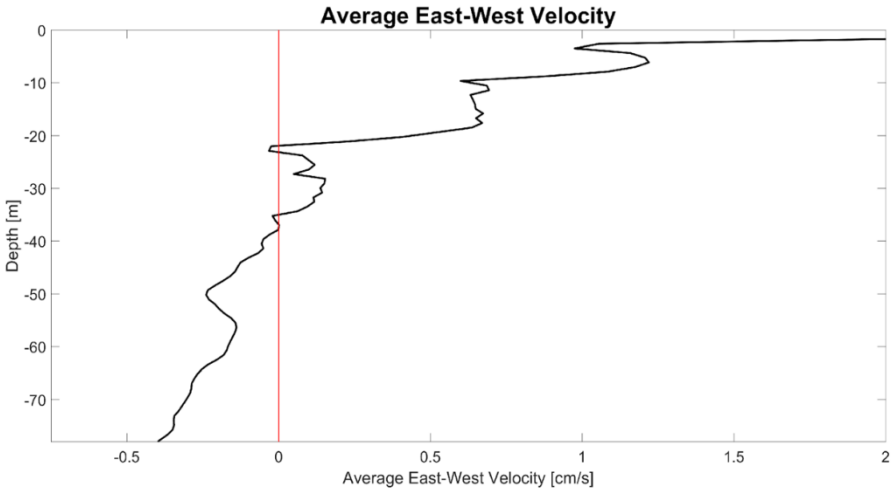

Figure 5.1.3: A time average of along-channel velocities for 2014 showing inflow above ~35 m and outflow below ~35 m. The vertical red line at velocity zero represents the transition between westward velocity (negative values) and eastward velocities (positive values). With westward directed river discharge, it would be expected to see net westward flow at the surface. However, a net eastward flow throughout the year indicates that there is another force affecting flow patterns, possibly wind.

Wind has been recorded as having the ability to induce currents, even if the induced current is opposite of typical flow (Winant, 2004; Wong, 1994; Valle-Levinson and Blanco, 2004; Patzert 1974). This implies that although water from Baker River is flowing out-fjord (westward) in Martinez Channel, eastward wind has the ability to induce an eastward current and thereby overpower (or redirect) the outflowing river

water. This interaction causes fresh surface water to be pushed to the head of the fjord, inducing a sloped surface. Ross et al., (2015) also found this pattern occurring in Martinez Channel with the ~6 months of available data from 2010. Based on Ross et al., (2015) and the flow profile shown in this study, it is likely that wind-driven circulation was present in 2014. To reinforce this finding, wind direction was investigated to determine if it was primarily directed in-fjord.

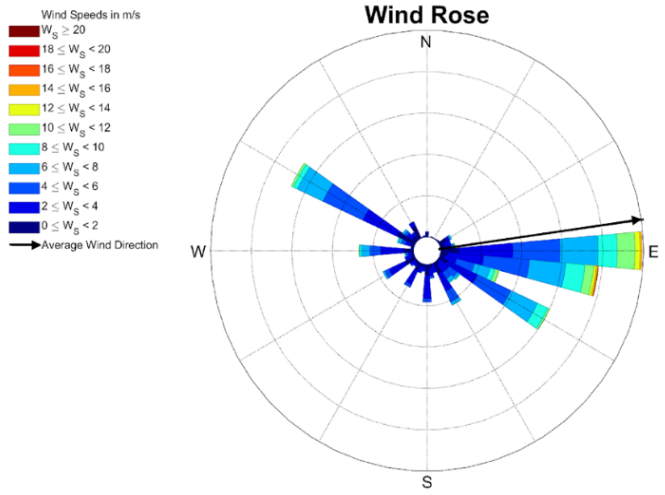

Figure 5.1.4: Wind rose showing wind velocity throughout 2014 with the average wind direction shown by the black arrow.

A wind rose reveals the dominant wind speeds and directions throughout 2014 (figure 5.1.4). These data show predominantly eastward winds with the yearly average wind directed east-northeastward (figure 5.1.4, black arrow). The primarily eastward wind could be reason for the net in-fjord surface flow shown in the time average along-channel velocity profile (figure 5.1.3), indicating that wind-driven circulation was influential in Martinez Channel in 2014.

In addition to driving circulation, Ross et al., (2015) also found that strong winds likely associated with the baroclinic annular mode (BAM) induced a deepening of the mixed layer in the fjord, which manifested as pycnocline depressions. The BAM is an atmospheric phenomenon similar to the North Atlantic Oscillation (NAO) and El Nino, yet occurs only in the southern hemisphere and has a periodicity of ~20-30 days (Thompson and Barnes, 2014). The BAM is characterized by eddy fluxes of heat that shed from the equator and move toward the southern pole (Thompson and Barnes, 2014), where these movements are driven by changes in temperature over increasing latitude. The propagation of the eddies, which manifest as low-pressure systems, or storms, gain strength by absorbing heat energy from the ocean or available body of water which increases moisture in the air and consequently precipitation (Ocean Today, 2011). The BAM manifests in Patagonia as a storm front with strong winds, warm air, and high precipitation propagating from west to east. The southern tip of South America is the only prominent land mass that protrudes into the Southern Ocean, implying that storm systems that propagate over Chilean Patagonia can produce strong onshore winds (>10 m/s). Onshore winds blowing into Martinez Channel tend to be particularly intense as the high-rising mountains bordering the channel directly funnel the winds from the storms from west to east, which allows them to gain strength from the surface water in the fjord (Ocean Today, 2011).

The echo anomaly shows that elevated winds associated with the BAM appeared to induce pycnocline depressions every ~20-30 days in Martinez Channel in accordance with what was found in Ross et al., (2015) (figure 5.1.5). Trends in the vertical location

of the pycnocline were compared to pulses in the lowpassed east-west current and wind velocities (showing trends occurring with a periodicity longer than five days) to investigate wind-induced flow and enhanced mixing at the pycnocline. Only along-fjord (east-west) winds were considered as the wind was predominantly eastward throughout 2014 (figure 5.1.4).

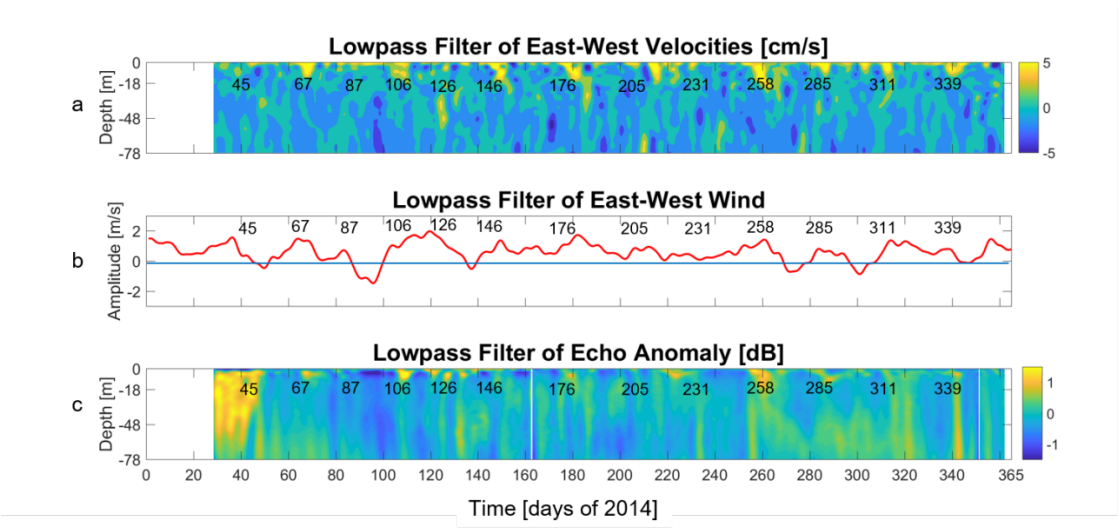

Figure 5.1.5: Lowpass filters removing trends less than five days of (a) along-channel velocity plotted with (b) smoothed along-channel wind velocity and (c) echo anomaly. Numerical indicators are placed on days of elevated signal in the echo anomaly, eastern wind, and eastern velocity. This figure is intended to compare the periodicity of these elevated signals with the BAM which manifests as high eastern winds every ~20-30 days in the southern hemisphere (Ross et al., 2015). This figure shows elevated signals every ~24.5 days on average, indicating that the BAM causes eastern surface flow and a depression of the pycnocline interface (shown as an elevated signal around ~12-15 m deep in subplot c).

The east-west velocities and echo anomaly showed simultaneous pulses in signal near the surface every ~20-30 days along with elevated eastern wind (figure 5.1.5). More specifically, an elevation in eastward surface velocities (> 5 cm/s) was seen at the same time as an elevated echo anomaly signal (> 0.5 dB) and occurred with an average periodicity of 24.5 days, which is within the range of the ~20-30 day periodicity of the BAM. The mechanics of wind-induced circulation resulting from the BAM support the idea of periodic pycnocline depression.

As previously mentioned, pycnocline depressions would appear as elevated signal(s) in the echo anomaly (Ross et al., 2015). To quantitatively identify whether these depressions occurred with the same periodicity as the BAM, a spectral analysis was done for the top 20 m of the water column. Figure 5.1.6 shows high energy (~ 1.45 dB^2/cpd^2) in the pycnocline region (~3-8 m) around 0.03-0.05 cycles per day (cpd; representing $\frac{1\ cycle}{30\ days}$ and $\frac{1\ cycle}{20\ days}$ respectively). This reaffirms that the storminess generated by the BAM influences variance in the fjord. The high energy (>1.5 dB^2/cpd^2) between 3 and 10 m depth from 0 cpd to ~0.03 cpd is likely indicative of seasonal variations ($\frac{1\ cycle}{96\ days}$ = 0.01 cpd). Figure 5.1.6 also shows a slight pulse of energy (1.4 dB^2/cpd^2) around 4 m depth that occurs at 0.07 cpd. This is likely variation due to the spring and neap tide cycles ($\frac{1\ cycle}{14\ days}$ =0.07 cpd).

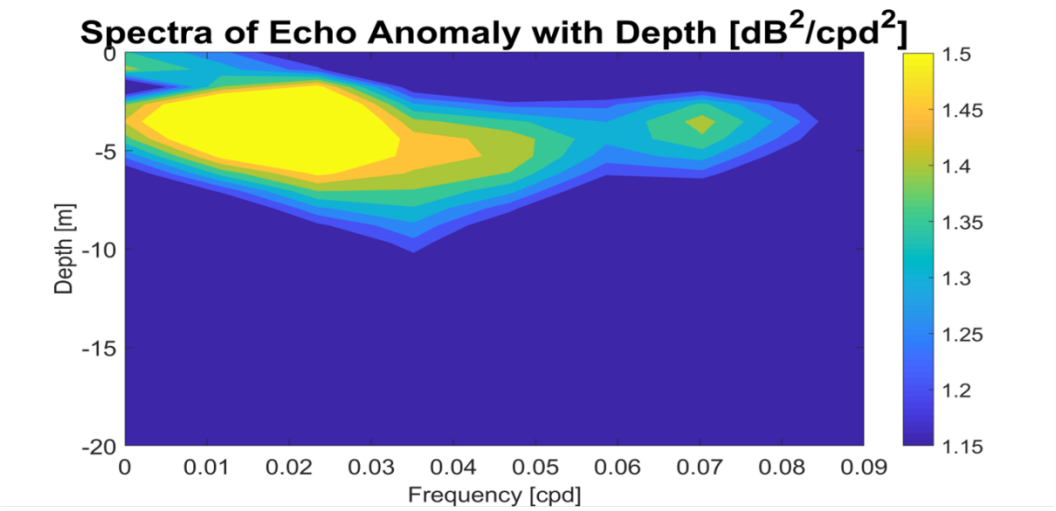

Figure 5.1.6: Spectral analysis on the echo anomaly for the top 20 m of the water column. This figure is intended to investigate whether variation in the echo anomaly matched the periodicity of the baroclinic annular mode (BAM; ~20-30 days or 0.03-0.05 cycles per day). The figure shows elevated signal (>1.4 dB^2/cpd^2) near the pycnocline (~3-8 m depth) which indicates that the BAM influences variance within the fjord. There is also elevated signal present around 0.01 cpd and 0.07 cpd which represent seasonal and fortnightly variations respectively.

Now that it has been shown that the BAM causes pycnocline depressions in the fjord, a theoretical quantification of the dissipation of Turbulent Kinetic Energy (TKE), denoted

ε, will be examined to explore the effect of wind on mixing in the surface layers of the fjord.

5.1.1 Investigation of Wind and Wave-Induced Mixing

To investigate whether wind or wave-driven mixing played a role in Martinez Channel, theoretical calculations of turbulence (TKE dissipation) based off measured wind values were performed following the method adapted from Csanady (1978). Wind stress on the surface was calculated using equation (5.1.1.1):

$$\tau = \rho_{air} * cd * u_{10}^2 \qquad (5.1.1.1)$$

where ρ_{air} is the density of air (0.0012 kg/m^3), *cd* is the drag coefficient, and u_{10} is the wind speed at 10 m from the water surface. The boundary layer velocity (u_*) was then calculated by dividing τ by the density of water at the surface (1002 kg/m^3 taken from the CTD at 2 m depth). Turbulent kinetic energy (TKE; ε) was found using the following equation (5.1.1.2) and gives an idea of turbulence in the water column:

$$\varepsilon = \frac{{u_*}^3}{k*z} \qquad (5.1.1.2)$$

where u_* is the boundary layer velocity, *k* is the Von-Karman Constant (0.41), and *z* is depth in m.

In addition to wind-driven mixing, fjords can experience mixing induced by waves (Bourgault and Kelley 2003). Therefore, the depth of influence of the surface waves generated by the wind was also calculated and explains how deep in the water column the surface waves can penetrate. It is calculated through a series of equations starting with (5.1.1.3) which calculates the boundary wind velocity, u_{*wind}:

$$u_{*wind} = \sqrt{cd} * sp \quad (5.1.1.3)$$

where *cd* is drag coefficient (as defined above) and *sp* is wind speed throughout the year. This value was then used in equation (5.1.1.4) to calculate the influence of the fetch on wind mixing, $\hat{x}$:

$$\hat{x} = \frac{g*x}{u_{*wind}{}^2} \quad (5.1.1.4)$$

where *g* is the acceleration due to gravity, *x* is the length of the surface affected by the wind (wind fetch; 15000 m), and u_{*wind} is the boundary layer velocity at the surface. Then, the period of the surface waves generated by the wind $\widehat{Tp}$ was calculated using equation (5.1.1.5) and plugged into equation (5.1.1.6) to find the last required input for the calculation of the depth of influence:

$$\widehat{Tp} = 0.751 * \hat{x}^{1/3} \quad (5.1.1.5)$$

$$L = \frac{g*(\widehat{Tp}*\frac{u_{*wind}}{g})^2}{2*\pi} \quad (5.1.1.6)$$

where L represents the wind induced wavelength and all other variables are defined as before. Finally, the depth of influence is calculated as half of the length of waves (assuming deep water waves; Dean and Dalrymple, 1991) and represents the depth that waves generated by the wind can reach and changes throughout the time series.

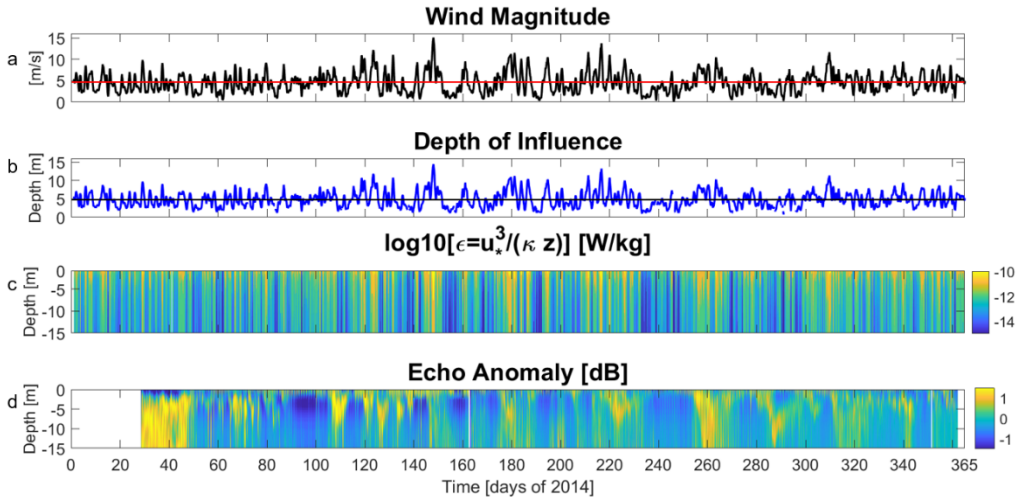

Figure 5.1.1.1: This figure is intended to investigate wave-induced mixing from waves generated by the BAM in Martinez Channel. To show this, (a) wind magnitude is plotted against (b) depth of influence (indicating how deep in the water column the wind affects), (c) turbulence, and (d) echo anomaly. It is hypothesized that in addition to inducing pycnocline depressions (seen as elevated signals in subplot d), wind induces turbulence (elevated signals in subplot c).

Previous studies have found that wind forcing can induce turbulence in fjords (Farmer and Freeland, 1983). Therefore, dissipation of TKE due to wind was plotted alongside wind magnitude and echo anomaly to qualitatively investigate if periods of pycnocline depression were due to wind induced mixing in the surface layer of the fjord. Figure 5.1.1.1 shows that turbulence is elevated at the BAM periodicity, which occurs concurrently with vertical depressions of the pycnocline. In addition to quantifying the TKE dissipation due to wind, the depth of influence of the waves generated by the wind was also quantified (figure 5.1.1.1b). The depth of influence of the waves indicates how deep in the water column the wind-driven waves penetrate the water column. It was found that during periods of sustained strong winds (day 150; >10 m/s; figure 5.1.1.1a), the depth of influenced reached ~15 m (figure 5.1.1.1b), which depressed the pycnocline (deepened the mixed layer; figure 5.1.1.1c). Overall, values of TKE dissipation quantified for this study (between 10^{-15} and 10^{-8} W/kg; figure 5.1.1.1c) were lower than the typical value of $3x10^{-7}$ W/kg found in the mixing layer (Perez-Santos, personal communication,

2018) and those found in Perez-Santos et al., (2014) which also studied Martinez Channel (10^{-10} to 10^{-4} W/kg; figure 5.1.1.2). However, the turbulence values reported in Perez-Santos et al., (2014) were in-situ measurements from the fjord as opposed to a theoretical calculation only including wind, and therefore represent TKE dissipation derived from all mechanisms (i.e. velocity shears, lateral flows, water column instabilities, etc.). This implies that wind, both from wind-driven flow and from wind-driven waves, contributes to turbulence in Martinez Channel, particularly during periods of increased winds or 'storminess' due to the BAM.

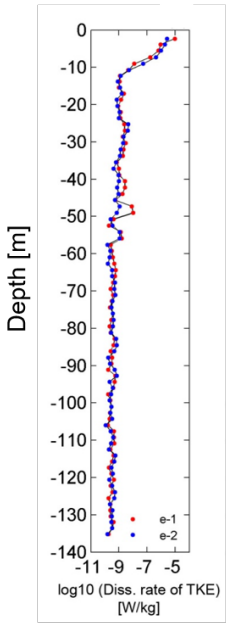

Figure 5.1.1.2: Turbulent Kinetic Energy dissipation values measured in Martinez Channel on January 28, 2014 at 16:07 (Perez-Santos, personal communication, 2018). Red and blue dots represent measurements from different devices.

The wind creates a wedge of freshwater that is deeper downwind (figure 5.1.1.3) which induces mixing near the surface and subsequently causes a deepening of the mixed layer. This manifests as pycnocline depressions and an elevation in echo anomaly signal between ~12-15 m deep. The ~20-30 day periodicity of this reinforces that the deepening is likely a result of the influence of the BAM which is consistent with BAM induced pycnocline depressions shown in Ross et al., (2015).

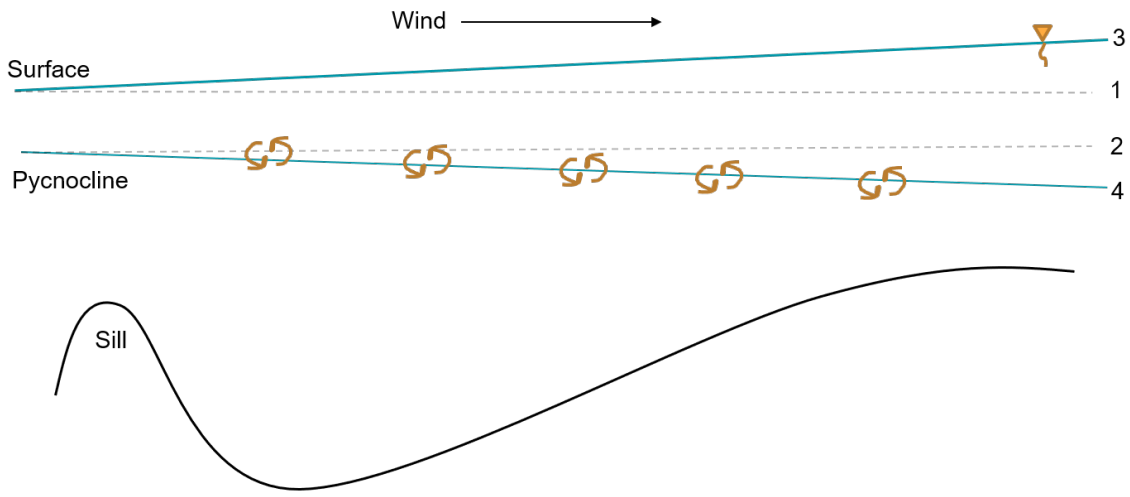

Figure 5.1.1.3: A general depiction of wind-driven pycnocline depression that causes a freshwater pile-up near the head of the fjord. Locations 1 and 2 represent the location of the surface and pycnocline without the presence of wind forcing respectively. Locations 3 and 4 depict the freshwater pile-up at the surface and the pycnocline depression respectively. Brown arrows show mixing of the deeper pycnocline location and the water surface is indicated by the inverted triangle on the right.

Regions of elevated turbulence in the water column have been shown to pose a boundary for the diel vertical migration (DVM) of zooplankton (Ianson et al., 2011; Farmer and Freeland 1983). To relate elevated TKE caused by the BAM to the DVM pattern in the fjord, volume backscatter patterns during pycnocline depression were analyzed.

5.2 Fjord Biology

In Martinez Channel, the combination of the elevated turbulence, sharp salinity gradient, and relatively high velocity at the pycnocline produces a physical upper barrier of DVM in Martinez Channel (Meerhoff et al., 2014). However, during periods of pycnocline depression induced by the BAM, this barrier deepens to ~12-15 m and both wind-induced and wave-induced turbulent dissipation occurs. This manifests as the strong signal over a small range of depth (~ 2 m at 8 m depth) at the pycnocline weakening over ~5 m and extending to ~12-15 m depth as the BAM induces mixing. An example of this is seen the

week of October 12th where the signal becomes weaker (~ -24 dB re 1 m^{-1}) and deeper (~12-15 m instead of ~8 m), indicating a deeper mixed layer, following the first day of the week when the wind associated with the BAM started to propagate (October 12th; figure 4.9.4). Studies have shown that increased mixing and consequently turbulence benefits predators by increasing their encounter rate with zooplankton (Pecseli et al., 2011), which is incentive for zooplankton to avoid turbulent areas. This indicates that the deepening of the mixed layer might deter zooplankton from migrating completely to the density interface. Also, mixing at the density interface supports the incorporation of nutrients into deeper water (Farmer and Freeland 1983), suggesting that full ascension to the pycnocline may not be necessary.

Diel migration patterns during a period of pycnocline depression in the week of October 12th, 2014 support this hypothesis. During this week, the pycnocline depresses from ~8 m to ~12-15 m and an elevated *Sv* signal (>-28 dB re 1 m^{-1}) consistent with DVM is found from sunset to sunrise most nights (figure 4.9.4). However, this signal only extends upwards to ~30 m rather than up to the pycnocline (~12-15 m) as seen in the other sample weeks of DVM occurrence (figure 4.9.1; figure 4.9.2; figure 4.9.3; figure 4.9.4). To emphasize this, the week of October 12th was plotted between 20 and 78 m depth to isolate the DVM signal and alter the color bar to see if there was any activity between ~20 and 30 m depth that the strong signal from the pycnocline was overpowering or saturating (figure 5.2.1). As expected, the cropped figure shows very little activity between 20 and ~30 m, indicating that the zooplankton did not fully ascend to the pycnocline as they did in other representative weeks throughout the year. This is

ostensibly due to the depression of the pycnocline and consequent widening of the mixed layer.

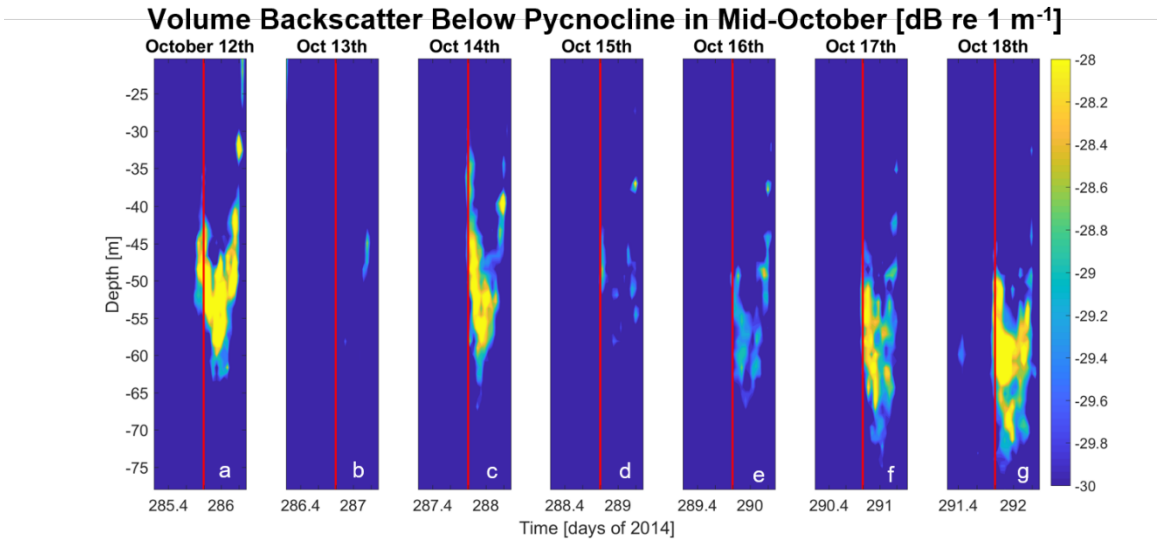

Figure 5.2.1: Volume backscatter plotted between the depressed pycnocline (20 m) and 78 m to isolate DVM signal and remove strong signal from the pycnocline to investigate if zooplankton made a full ascension to the depressed pycnocline. Sunset times are denoted by vertical red lines and sunrise times separate subplots a-g. DVM pattern does not extend upwards of 30 m, indicating that zooplankton do not fully ascend to the pycnocline during periods of pycnocline depression.

To investigate how biology interacts with the BAM over the entire time series, a depth average of volume backscatter was taken between 20 and 78 m to isolate signals associated with the DVM and disregard signal from the pycnocline region. This allows for direct comparison of DVM signal during periods of pycnocline depression and otherwise. Figure 5.2.2 shows a depth average of volume backscatter (between 20 and 78 m) during periods of BAM storminess (illustrated by the numerical indicators) to explore how the DVM pattern is affected by pycnocline depressions. Above-average volume backscatter during periods of BAM influence indicate that this phenomenon likely increases DVM in Martinez Channel. To further affirm this, an average of depth and time was taken during periods of pycnocline depression and compared to the depth and time

average of the rest of the year. The depth and time average volume backscatter signal between 20 and 78 m depth for the days with enhanced winds and waves due to the BAM was -32.98 dB re 1 m^{-1} compared to -33.88 dB re 1 m^{-1} for the days of 2014 featuring nominal conditions. This slightly higher signal suggests that the BAM might increase DVM. However, this finding warrants further investigation, especially because it is unknown whether the number of zooplankton migrating would increase or if the frequency of migration during the BAM increases.

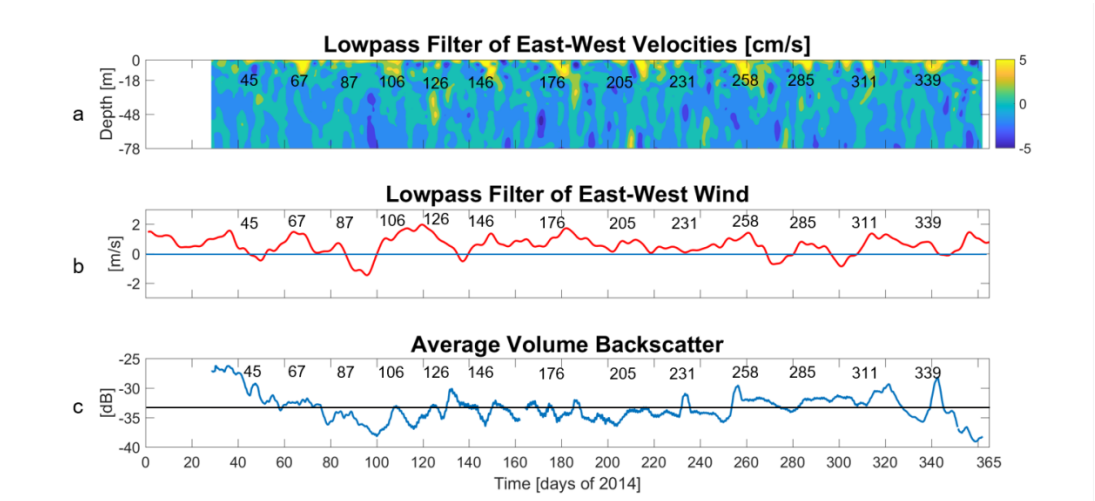

Figure 5.2.2: This figure is intended to investigate trends in how the average volume backscatter responds during periods of pycnocline depressions induced by the BAM that propagates ~20-30 days indicated by the numerical indicators on each subplot. In 2014, propagation of the BAM was seen an average of 24.5 days. Lowpass filter removing trends less than five days of the (a) along-channel velocity and (b) along-channel wind plotted with (c) a depth average of volume backscatter between 20 m and 78 m. These depths disregard the pycnocline and allows for direct comparison of average diel vertical migration patterns with depressions of the pycnocline induced by high eastern winds. The blue line at 0 m/s in subplot b represents a change in wind direction with positive values representing eastward wind and negative representing westward. The black line in subplot c at -33.35 dB represents the average volume backscatter value between 20-78 m for the entire year and is intended for reference.

In addition to being influenced by sunlight, zooplankton migrations have also been shown to be affected by variation in moonlight availability (Alldredge and King 1980). Alldredge and King (1980) conducted a study on a subtidal sand flat in the Gulf of California, Mexico that explored the effect of light on DVM, particularly light associated with the lunar cycle. Migrations to the pycnocline are expected to decrease during highly-lit periods (i.e. full moons) so zooplankton avoid visible predation at the surface. This study found polychaetes, amphipods, copepods, and isopods among other zooplankton

species when sampling 2 h periods once every 24 h for four days. This sampling method was repeated for new, full, first, and last-quarter moons for July and August of 1978. The study concluded that copepod migration was not significantly influenced by moonlight but migration of polychaetes and larger amphipods was.

Monthly in-situ zooplankton sampling carried out in Martinez Channel in every month of 2010 also found polychaetes, amphipods, and copepods, the latter being the most abundant on the magnitude of 10^5 per 100 m^3 of water. Distribution of the zooplankton from 2010 is shown in figure 5.2.3.

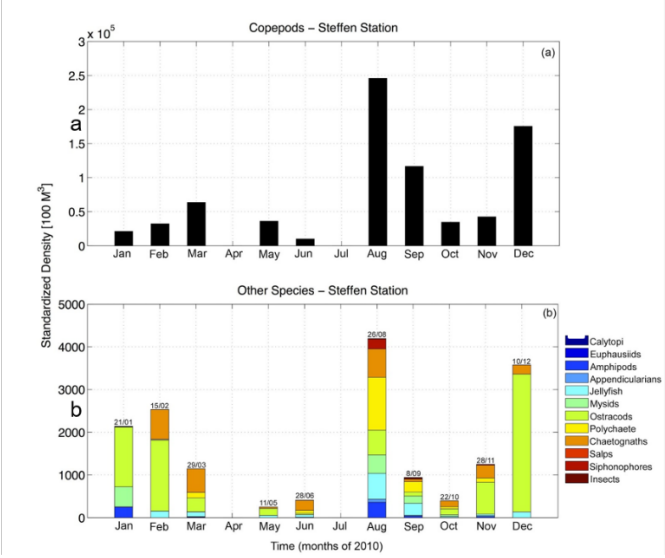

Figure 5.2.3: Distribution of zooplankton species recorded in 2010 from Ross et al., (2015 IEEE). The figure indicates that (a) copepods dominated species distribution compared to (b) other species. The figure also shows that August contained the highest quantity of zooplankton followed by December. Figure adapted from Ross et al., (2015).

These findings are the most recent data available for Martinez Channel and therefore provide a general idea of zooplankton species distribution. As copepods were most abundant (figure 5.2.3a), their migration pattern is likely to be representative of the overall migrations patterns in Martinez Channel. Alldredge and King (1980) found

copepod migration was not significantly influenced by moonlight and occurred consistently at dusk. Valle-Levinson et al. (2014) also found moon phase to have limited influence on copepod migration. Therefore, it is likely that the DVM pattern in Martinez Channel did not vary throughout the lunar cycle as copepods dominated the species distribution. However, some variation depending on moonlight availability is possible as other species found in Martinez Channel such as polychaetes and larger amphipods have been shown to decrease their migration during moonlit periods to reduce visible predation (Alldredge and King 1980).

Visible predation is most threatening during full moons and least threatening during new moons. This is because full moons increase visibility within the water column, making it easier for predators to see the zooplankton migrating, and new moons produce the least amount of light which masks the zooplankton migration from predators. Therefore, volume backscatter (*Sv*) signal was compared for full moon periods versus new moon periods to investigate if more zooplankton migrated during new moons, indicated by a higher signal in *Sv*. This was done by taking the maximum *Sv* signal between 20 and 78 m (between the deepest depressed pycnocline depth and deepest recorded data point) during each full moon and new moon and averaging them respectively (figure 5.2.4). Contrary to expected, the average signal for full moon migration was larger than the average for new moon migration (-21.49 dB re 1 m^{-1} compared to -23.77 dB re 1 m^{-1} for new moons).

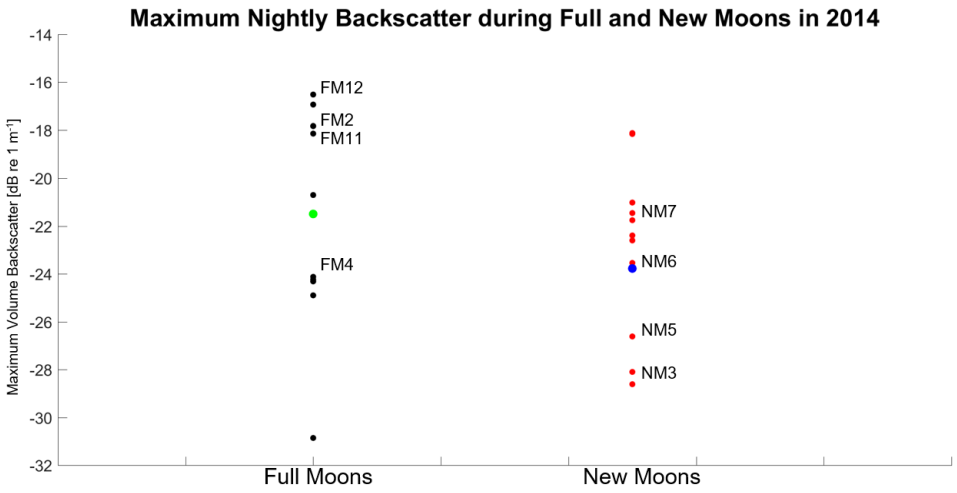

Figure 5.2.4: Maximum volume backscatter between 20 and 78 m depth during full moons versus new moons throughout 2014. Theoretically, nightly zooplankton migrations are expected to be greater during new moons as there is less risk of visible predation than during full moons. For easier comparison, the total average volume backscatter during full moons (the green dot) was calculated alongside the total average volume backscatter during new moons (the blue dot). The labeled moons represent periods when the BAM propagated. For full moons, this occurred on February 14th, April 15th-16th, November 6th-7th, and December 5th-6th, 2014 (FM2, FM4, FM11, and FM 12 respectively). For new moons, it was March 28th-30th, May 26th-28th, June 25th-27th, July 24th-26th, 2014 (NM3, NM5, NM6, and NM7 respectively).

However, four new moons in 2014 (January 1st and 30th, November 22nd, December 2st) occurred during periods where the DVM pattern did not qualitatively appear in the *Sv* (before April 1st and after November 14th, 2014). The lack of DVM pattern might be due to limited food source. This is due to Chlorophyll measurements from November and December showing lower values than measurements recorded in January and June (<~0.1 CCI compared to ~0.2 CCI for January and June casts; figures 4.2.1 and 4.2.2). Chlorophyll is a representative measurement of primary producers, implying that food availability for zooplankton was low during these periods and therefore factored into the migration pattern more-so than the moon phase. The DVM pattern appears to have faded around November 14th (figure 4.8.2), indicating that food levels might be decreased around this time. The next available chlorophyll measurement (November 29th) showed values <~0.005 CCI above the pycnocline, indicating a limited supply of food.

Another reason for an elevated DVM pattern during full moons could be the overlap between full moons and BAM influence. This occurred on February 14th, April 15th-16th, November 6th-7th, and December 5th-6th in 2014 (figure 4.8.1; figure 4.8.2) which represent the second, fourth, eleventh, and twelfth full moon respectively (FM2, FM4, FM11, FM12; figure 5.2.4). The maximum volume backscatter during these times was -17.84, -24.12, -18.15, and -16.52 dB re 1 m^{-1} respectively, indicating that the mixing generated by the BAM might cause an increase in DVM despite the light from the full moon. However, based on this hypothesis, it would be expected to see an increase in *Sv* during periods when new moons and the BAM-induced storms overlap as well. To the contrary, results show that the maximum *Sv* during periods of BAM influence and new moons were less than periods when BAM influence overlapped full moons (figure 5.2.4). This indicates that something external to these factors may be causing the increase of DVM during full moons and/or the decrease of DVM during new moons. It is important to remember that the BAM is a proxy for storminess in the southern hemisphere that brings high winds, low pressure, and elevated moisture (Ross et al., 2015). The elevated DVM signals during the full moons when the BAM influence was present could be due to an increase in cloud cover in addition to the increased turbulence near the surface.

To investigate whether cloud cover affected DVM patterns in 2014, weather was analyzed for the period when the BAM overlapped with full moons and new moons (World Weather Online). On average, the full moons had a cloud cover of 43.33% at 7:00 pm (around sunset) whereas new moons had 33.25% cloud cover. Averages were calculated by averaging the values for each full moon period. The additional cloud cover

during the four full moons that occurred concurrently with a storm could contribute to the high values of volume backscatter during these times by limiting moonlight.

This study was able to conclude that overall, the lunar cycle seemed to have little effect on DVM in Martinez Channel. This aligns with Valle-Levinson et al., (2014) and Alldredge and King (1980) who found light availability from the lunar cycle to bear little effect on copepod migration, the most abundant species in Martinez Channel according to Ross et al., (2015). Also, the BAM appeared to increase DVM but limited the upward migration to ~30 m instead of fully to the pycnocline (which is ~12-15 m during depression). To expand on the findings of this study, future studies should include in-situ sampling of zooplankton species, age, and sex, chlorophyll levels throughout the year, and temperature variation with depth to obtain a full picture of intra-annual migration patterns in Martinez Channel. In addition, having in-situ samples during periods where *Sv* is quantified would allow for a more accurate description of species migration patterns. Next, this study investigates how a GLOF relates to the biology and how these are both affected by the BAM.

5.3 Glacial Lake Outburst Flooding

Glacial Lake Outburst Floods (GLOFs) have been found to influence the abundance and composition of biology by delivering high concentrations of suspended sediments (Meerhoff et al., 2014). As a DVM pattern persisted through most of 2014 in Martinez Channel, it is important to investigate how the GLOF interacted with this pattern. A model created by Marin et al., (2013) to investigate impacts of GLOFs on suspended sediment concentration in the Baker-Martinez fjord complex found that an influx of

glacial flour (glacial sediments) resulting from a GLOF increased suspended solid concentrations by 240 times at the head of Martinez Channel (Marin et al., 2013). High concentrations of suspended sediments have been shown to decrease primary production (Meerhoff et al., 2014; Montecino and Pizarro, 2008), subsequently decreasing secondary production (i.e. zooplankton). This indicates that suspended sediments delivered by a GLOF might decrease DVM of zooplankton by reducing their food source, phytoplankton.

However, the 2014 GLOF in Martinez Channel occurred during mid-to-late summer when primary producer concentrations are typically limited (Meire et al., 2017; Walker, 2000). Consequently, zooplankton have less reason to migrate vertically during this time as food isn't as readily available and surface temperatures are higher (Meerhoff et al., 2014; Valle-Levinson et al., 2014). Therefore, there was no DVM pattern present during the GLOF and decreased DVM pattern after November 14th, as this is when surface temperatures begin warming and primary production would decrease (figure 4.8.1; figure 4.8.2). This is evident from a lack of vertical pattern in both the echo anomaly and volume backscatter from November 14th to April 1st (figure 4.8.1; figure 4.8.2). If the GLOF occurred during a time that DVM was present, it would be likely to see the pattern halted or obscured as reported in Ross et al. (2015). However, Ross et al. (2015) also reported a positive correlation (r^2=0.74) between increases in river discharge and *Sv*, indicating that large scatterers (>5 mm) are present within the water column. In addition, Ross et al. (2015) showed an elevated *Sv* (> -80 dB re 1 m^{-1}) signal during the GLOF which is to be expected (Marín et al., 2013). However, this strong signal persisted from

days 28-50 (January 28th- February 19th) although the GLOF occurred during days 32-34 (February 1st-3rd). It is unknown why there would be an elevated signal preceding the GLOF. No other extreme events that could lead to increased concentrations of sediment such as a landslide were reported before February 1st (the date of the GLOF).

As addressed in Section 5.1, Martinez Channel showed wind-driven circulation in 2014. During the GLOF and shortly thereafter, wind and surface velocities were directed eastward (in-fjord; figure 4.4.3; figure 4.3.1). The elevated wind showed BAM periodicity (~20-30 days) and was directed predominantly eastward for the first 50 days of 2014 (until day February 19th; figure 5.3.1). Figure 5.3.1 shows lowpass wind and velocity for the days surrounding the GLOF (day 30-36; January 30th-February 5th). The eastward surface flow occurring in conjunction with eastward wind implies that the wind driven flow was significant enough to retain flood waters near the head of the fjord. However, there wasn't a significant westward return flow observed (figure 4.4.2; figure 4.4.3). This could be due to wind spreading the water out over a large surface area and preventing a concentrated westward return flow. An investigation into differences between GLOFs occurring during periods of wind-forcing versus periods of wind dormancy would be beneficial as the BAM and GLOFs are both significant phenomena occurring in Martinez Channel.

Retention of floodwaters could have important implications for local biology as fjords are highly productive marine ecosystems. The elevated signal in the *Sv* persisted for ~20 days after the GLOF occurred (figure 4.8.1), indicating that the wind from the BAM could

retain floodwaters and sediment contained within. Sediment retained near the shore could potentially settle in high concentrations and bury marine nurseries rather than dispersing down-fjord, hindering marine populations. Also, new terrigenous substances introduced by the GLOF could interact with existing biology in the fjord and influence symbiotic relationships. Unfortunately, this study did not focus on the organic composition of glacial flour brought in by a GLOF and therefore this is beyond the scope of this study.

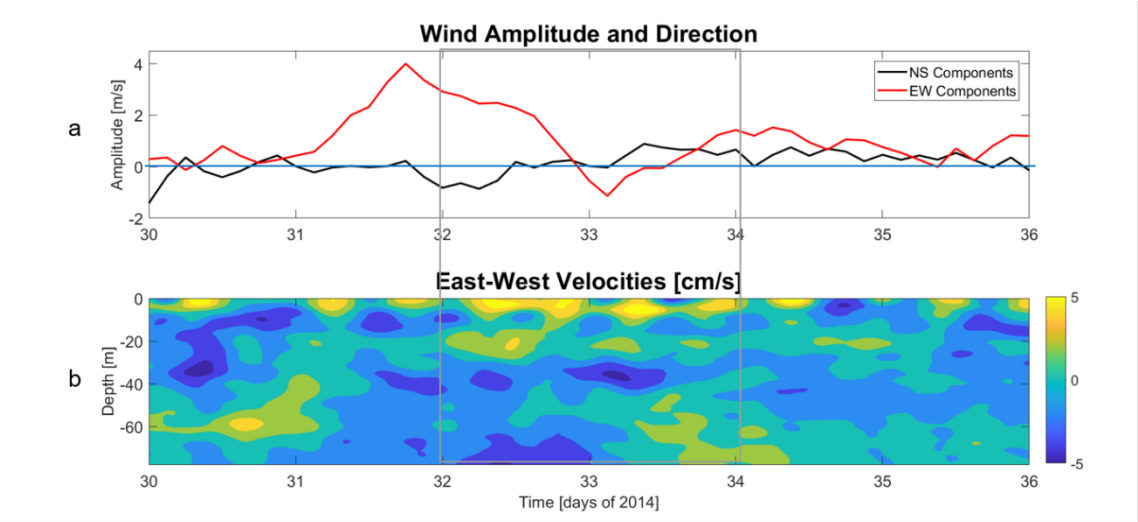

Figure 5.3.1: (a) Filtered wind data showing north and east directions above the blue line and south and west below and (b) along-channel velocities surrounding the GLOF occurring between days 32-34 (shown in the gray box). This figure is intended to compare wind influence on flow direction.

It is important to understand how GLOFs interact with the physics and biology of Martinez Channel to get a full picture of what happens during these increasingly frequent events. From this study, it is inferred that winds associated with the BAM are capable of retaining floodwaters from a GLOF at the head of the fjord and that GLOF sediment influx could potentially reduce primary production and consequently secondary production by decreasing light availability.

Although the data analyzed in this study provides a good description of Martinez Channel through 2014, it is important to understand the limitations of the above-mentioned

analyses. Therefore, the following section discusses the limitations affecting this study that could ideally be improved upon in future work.

STUDY LIMITATIONS

Unfortunately, this study was not without limitations. Perhaps the biggest limitation in investigating the role of the BAM on fjord circulation was that the closest available wind measurements were ~100 km away from where the ADCP was moored in Martinez Channel (figure 3.1). However, both locations are under the influence of the westerlies and therefore exhibit similar wind patterns, making the wind collection location an acceptable proxy for wind through Martinez Channel.

Another limitation to this study is the complex geometry of the fjord. Specifically, fjord bathymetry and elevation can affect flow patterns (Gille, 2003). To ensure comprehensiveness in future studies, fjord bathymetry and elevation should be considered. In addition, the location of the ADCP mooring was at a very complex location in the fjord, as it was at the junction of Martinez Channel and Stefan Fjord (figure 2.1). Future studies could benefit from ADCPs moored at several locations along Martinez Channel concurrently to determine which system (Stefan Fjord or Martinez Channel) has more influence over fjord circulation. However, the difficulty of mooring instruments in this remote part of the world would make this a difficult feat.

Future studies linking physical and biological characteristics of this system would benefit from investigating the role of zooplankton within Martinez Channel as there was shown to be a correlation between zooplankton DVM patterns and the BAM. In-situ sampling of zooplankton species, age, and sex distributions as well as measurements of primary producers in the fjord throughout the year would complement the ADCP measurements.

CONCLUSION

The purpose of this study was to characterize intra-annual variations in fjord hydrodynamics and biology and to determine how these change in the presence of a GLOF. Wind was found to have a major influence on the fjord hydrodynamics and should be considered in future studies. Specifically, wind was found to drive circulation through most of 2014 and wind associated with the BAM induced enhanced TKE dissipation which resulted in a depression of the pycnocline every ~20-30 days. Ross et al., (2015) recognized this pattern persisting for three months in Martinez Channel. However, a study observing this pattern for an entire year has never been conducted before. Therefore, the year-round pycnocline depressions induced by the BAM found in this study represent a novel finding for this region and suggest that the BAM could play a role in other Chilean Patagonian fjords.

Considering that South America can be expected to experience an increase in GLOF events (Dussaillant, 2009; Harrison et al., 2006; Ross et al., 2015), understanding the interaction between the BAM and GLOFs is important. This study showed that winds from the BAM were prominent enough to retain floodwaters associated with a GLOF at the head of the fjord. This can have major implications for local marine life as GLOFs deliver a lot of suspended sediment into fjord systems (typically increasing existing concentrations by a factor of 240). The high echo anomaly signal persisting ~20 days after the GLOF event suggests that suspended sediment is retained along with the floodwaters. This means that suspended sediment is likely to settle in one concentrated

location instead of dissipating over the length of the fjord which can shroud marine life and negatively affect benthic communities. The retention of glacial flour delivered by a GLOF could also negatively affect DVM in Martinez Channel by hindering light availability for primary production. Unfortunately, the GLOF in this study occurred during a period where DVM wasn't present. Therefore, this suggestion warrants further investigation.

In addition to investigating light availability associated with sediment from a GLOF, this study also considered variation in light availability due to the lunar cycle. Although this study suggests that the lunar cycle did not affect DVM, it is difficult to make a conclusion as biology is influenced by many factors that this study was not able to account for. For example, factors such as food availability, light availability, and zooplankton species, sex, and age distribution affect the DVM pattern so measurements of these would ensure a more comprehensive study on the DVM of zooplankton (Valle-Levinson et al., 2014). However, this study was able to conclude that the average maximum migration signal from the volume backscatter was higher for full moons throughout 2014 as opposed to new moons. Unfortunately, it is not possible to determine whether this is a result of an increase in the number of zooplankton migrating or an increase in the frequency of migrations with the available data. In-situ measurements of zooplankton at different depths during periods of quantified volume backscatter could assist in forming a more confident conclusion regarding the effect of moon phase on DVM in Martinez Channel.

Overall, this study was able to characterize the effects of external events such as the BAM and GLOFs on fjord physics and biology in Martinez Channel by using a comprehensive data set encompassing 2014. This study provides a basis of knowledge for comparing future conditions of Martinez Channel to evaluate the effects of climate change.

BIBLIOGRAPHY

Aiken, C.M. "Seasonal thermal structure and exchange in Baker Channel, Chile." *Dynamics of Atmospheres and Oceans* 58 (2012): 1-19. Print.

Alldredge, A.L., King, J.M. “Effects of moonlight on the vertical migration patterns of demersal zooplankton.” *Journal of Experimental Marine Biology and Ecology*, vol. 44, no. 2, 1980, pp. 133–156., doi:10.1016/0022-0981(80)90150-1.

Barnett, T. P. "Interaction of the monsoon and Pacific trade wind system at interannual time scales." *Deep Sea Research Part B. Oceanographic Literature Review* 30.12 (1983): 912. Web. 27 June 2017.

Bennett, C. "Chile to warm up its renewables market." *Renewable Energy Focus* 9.7 (2009): 79-83. Web.

Bourgault, Daniel, Kelley, D.E. “Wave-Induced boundary mixing in a partially mixed estuary.” *Journal of Marine Research*, vol. 61, no. 5, Jan. 2003, pp. 553–576., doi:10.1357/002224003771815954.

Brown, J., Colling A., Park D., Phillips J., Rothery, D., Wright, J. *Waves, tides and shallow-water processes: prepared by an open university course team*. Ed. Gerry Bearman. Oxford : Milton Keynes: Pergamon ; Open U, 1989. Print.

Burrall, K., Leandro G., Mar L., Natale E., Tauro, F. "Analysis of Proposed Hydroelectric Dams on the Río Baker in Chilean Patagonia." *Massachusetts Institute of Technology: Department of Civil and Environmental Engineering* (2009): 1-36. Web.

Cabrer, R., Deines, K., Brumley, B., Terrey, E., “Development of a Practical Coherent Acoustic Doppler Current Profiler.” *Oceans 87*, 1987, doi:10.1109/oceans.1987.1160903.

“Colonia Glacier Retreat and Glacier Lake Outburst Floods.” *From a Glaciers Perspective*, 16 Mar. 2014, glacierchange.wordpress.com/2011/03/24/colonia-glacier-retreat-and-glacier-lake-outburst-floods/.

Csanady, G. T. “Turbulent interface layers.” *Journal of Geophysical Research*, vol. 83, no. C5, 1978, p. 2329., doi:10.1029/jc083ic05p02329.

Çengel, Yunus A., Cimbala, J.M. *Fluid mechanics: fundamentals and applications*. Third ed. New Delhi: McGraw-Hill Education, 2014. Print.

Dallas, G.M. "Principal Component Analysis 4 Dummies: Eigenvectors, Eigenvalues and Dimension Reduction." *George Dallas UK based Information Engineer/Internet Social Scientist*. N.p., 27 Jan. 2015. Web. 06 July 2017.

Dean, R.G., and Dalrymple, R.A. "Introduction to Wave Mechanics." *Advanced Series on Ocean Engineering Water Wave Mechanics for Engineers and Scientists*, 1991, pp. 1–5., doi:10.1142/9789812385512_0001.

Dewar, W. K., Bingham R.J., Iverson R.L., Nowacek D.P., St. Laurent, L.C. and Wiebe P.H. "Does the marine biosphere mix the ocean?" *Journal of Marine Research* 64.4 (2006): 541-61. Web.

Dushaw, B. "The HOME Farfield Experiment." *HOME: Farfield*, (2003) staff.washington.edu/dushaw/HOME/barotropic.html.

Dussaillant, A., Benito, G., Buytaert, W., Carling, P., Meier, C., Espinoza, F. "Repeated glacial-lake outburst floods in Patagonia: an increasing hazard?" *Natural Hazards* 54.2 (2009): 469-81. Web.

Dyer, K. R. *Estuaries: a physical introduction, 2nd edition*. 2nd ed. Chichester: John Wiley & Sons, 1997. Print.

Emery, W. J., Thomson, R.E. *Data analysis methods in physical oceanography*. Third ed. Kidlington: Elsevier, 2014. Print.

Evans, S. M. "Behavior in Polychaetes." *The Quarterly Review of Biology*, vol. 46, no. 4, 1971, pp. 379–405., doi:10.1086/407004.

Farmer, D.M., Freeland, H.J. "The physical oceanography of fjords." *Progress in Oceanography*, vol. 12, 1983, pp. 147–220.

Glasser, N. F., Harrison, S., Jansson, K.N., Anderson, K., Cowley, A. "Global Sea-Level Contribution from the Patagonian Icefields since the Little Ice Age Maximum." *Nature Geoscience*, vol. 4, no. 5, 2011, pp. 303-307.

Gille, S.T. "Bathymetry and Ocean Circulation." *Charting the secret world of the ocean floor; The GEBCO Project*, 2003.

Glick, D., Photograph by Warne, K."Sea Level Rise." *National Geographic*, 7 Apr. 2017, www.nationalgeographic.com/environment/global-warming/sea-level-rise/.

Greene, C., Wiebe, P. "Bioacoustical Oceanography: New Tools for Zooplankton and Micronekton Research in the 1990s." *Oceanography*, vol. 3, no. 1, 1990, pp. 12–17., doi:10.5670/oceanog.1990.15.

Harrison, S., Glasser, N., Winchester, V., Haresign, E., Warren, C., Jansson, K. “A Glacial Lake Outburst Flood Associated with Recent Mountain Glacier Retreat, Patagonian Andes.” *The Holocene*, vol. 16, no. 4, 2006, pp. 611–620., doi:10.1191/0959683606hl957rr.

Haury, L.R., Yamazaki, H., Itsweire, E.C. “Effects of turbulent shear flow on zooplankton distribution.” *Deep-Sea Research*, Vol. 37, no. No. 3, 23 Oct. 1989, pp. 447–461.

Huntley, M., Zhou, M. "Influence of animals on turbulence in the sea." *Marine Ecology Progress Series* 273 (2004): 65-79. Web.

Ianson, D., Allen, S.E., Mackas, D.L., Trevorrow, M.V., Benfield, M.C. “Response of Euphausia pacifica to small-Scale shear in turbulent flow over a sill in a fjord.” *Journal of Plankton Research*, vol. 33, no. 11, Apr. 2011, pp. 1679–1695., doi:10.1093/plankt/fbr074.

Inall, M.E., Gillibrand, P. A. “The physics of mid-Latitude fjords: a review.” *Fjord Systems and Archives*, vol. 344, 2010, pp. 17–33.

Macdonald, R.K. “Turbidity and light attenuation in coastal waters of the Great Barrier Reef.” *James Cook University*, 12 Oct. 2016.

Marín, V.H., Tironi, A., Parades, M.A., Contreras, M. “Modeling suspended solids in a Northern Chilean Patagonia glacier-Fed fjord: GLOF scenarios under climate change conditions.” *Ecological Modelling*, vol. 264, 2013, pp. 7–16., doi:10.1016/j.ecolmodel.2012.06.017.

Markert, R.E., Markert, B.J., Vertrees, N.J. “Lunar Periodicity in Spawning and Luminescence in Odontosyllis Enopla.” *Ecology*, vol. 42, no. 2, 1961, pp. 414–415., doi:10.2307/1932096.

Marshall, G.J., Thompson, D.W.J., van den Broeke, M.R. “The signature of Southern Hemisphere atmospheric circulation patterns in Antarctic precipitation.” Geophysical Research Letters, 44, 11,580-11,589. doi:10.1002/2017GL075998.

Meerhoff, E., Tapia, F.J., Sobarzo, M., Castro, L.R. “Influence of estuarine and secondary circulation on crustacean larval fluxes: a case study from a Patagonian fjord.” *Journal of Plankton Research*, vol. 37, no. 1, 2014, pp. 168–182., doi:10.1093/plankt/fbu106.

Meerhoff, E., Tapia, F.J., Castro, L.R. “Spatial structure of the meroplankton community along a Patagonian fjord – The role of changing freshwater inputs.” *Progress in Oceanography*, vol. 129, 2014, pp. 125–135., doi:10.1016/j.pocean.2014.05.015.

Meerhoff, E., Tapia, F.J., Castro, L.R., Sobarzo, M. “Estuarine circulation in the Baker/Martinez fjord complex, Chilean Patagonia, during the maximum river outflow season: implications for the transport of crustacean larvae.” *17th Physics of Estuaries and Coastal Seas (PECS) conference,* Porto de Galinhas, Pernambuco, Brazil (2014)

Meire, L., Mortenson, J., Meire, P., Juul-Pedersen, T., Sejr, M.K., Rysgaard, S., Nygaard, R., Huybrechts, P., Meysmen F.J.R. “Marine-terminating glaciers sustain high productivity in Greenland fjords.” *Global Change Biology*, 4 Aug. 2017, onlinelibrary.wiley.com/doi/10.1111/gcb.13801/full.

Montecino, V., Pizarro, G., Baker, C., Fallos, C. “Primary productivity, biomass, and phytoplankton size in the austral Chilean channels and fjords: spring–summer patterns.” *Progress in the Oceanographic Knowledge of Chilean Interior Water* (2008), pp. 93–97, Puerto Montt to Cape Horn. Comité Oceanográfico Nacional-Pontificia Universidad Católica de Valparaíso.

“Moon Phases 2014 – Lunar Calendar for Santiago, Chile.” *Timeanddate.com*, www.timeanddate.com/moon/phases/chile/santiago?year=2014.

Nash, J. D., Moum, J. N. River plumes as a source of large-amplitude internal waves in the coastal ocean. *Nature* (2005)*„ 437*(7057), 400-3. Retrieved from http://www.library.umaine.edu/auth/EZProxy/test/authej.asp?url=http://search.proquest.com.prxy4.ursus.maine.edu/docview/204573488?accountid=14583

Niklitschek, E.J., Soto, D., Lafon, A., Molinet, C., Toledo, P. "Southward expansion of the Chilean salmon industry in the Patagonian Fjords: main environmental challenges." *Reviews in Aquaculture* 5.3 (2013): 172-95. Web.

Palmer, J. "Chiles glacial lakes pose newly recognized flood threat." *Science* 355.6329 (2017): 1004-005. Web.

Pantoja, S., Iriarte, J.L., Daneri, G. "Oceanography of the Chilean Patagonia." *Continental Shelf Research* 31.3-4 (2011): 149-53. Print.

Patzert, W.C. “Wind-Induced reversal in Red Sea circulation.” *Deep Sea Research and Oceanographic Abstracts*, vol. 21, no. 2, 1974, pp. 109–121., doi:10.1016/0011-7471(74)90068-0.

Pécseli, H. L., Trulsen, J.K., Fiksen, Ø. “Predator-Prey encounter and capture rates in turbulent environments.” *Limnology and Oceanography: Fluids and Environments*, vol. 4, no. 1, 2014, pp. 85–105., doi:10.1215/21573689-2768717.

Pelto, M.S. “Colonia Glacier Retreat and Glacier Lake Outburst Floods.” *From a Glacier's Perspective*, 24 Mar. 2011, glacierchange.wordpress.com/2011/03/24/colonia-glacier-retreat-and-glacier-lake-outburst-floods/.

Pepper, R.E., Jaffe, J.S., Variano, E., Koehl, M.A.R. “Zooplankton in flowing water near benthic communities encounter rapidly fluctuating velocity gradients and accelerations.” *Marine Biology*, vol. 162, no. 10, 2015, pp. 1939–1954., doi:10.1007/s00227-015-2713-x.

Pérez-Santos, I., Garcés-Vargas, J., Schneider, W., Ross, L., Parra, S., Valle-Levinson, A. "Double-diffusive layering and mixing in Patagonian fjords." *Progress in Oceanography* 129 (2014): 35-49. Print.

Piret, L., Bertrand, S., Vandekerkhove, E., Harada, N., Moffat, C., Rivera, A. "Gridded bathymetry of the Baker-Martinez fjord complex (Chile, 48°S) v1." *Figshare*, 9 Sept. 2017, figshare.com/articles/Gridded_bathymetry_of_the_Baker-Martinez_fjord_complex_Chile_48_S_v1/5285521.

Postel, L., da Silva, A.J., Mohrholz, V., Lass, H. "Zooplankton biomass variability off Angola and Namibia investigated by a lowered ADCP and net sampling." *Journal of Marine Systems*, vol. 68, no. 1-2, 2007, pp. 143–166., doi:10.1016/j.jmarsys.2006.11.005.

Rivera, Andrés, Benham, T., Casassa, G., Bamber, J., Dowdeswell, A.J. "Ice elevation and areal changes of glaciers from the Northern Patagonia Icefield, Chile." *Global and Planetary Change*, vol. 59, no. 1-4, 2007, pp. 126–137., doi:10.1016/j.gloplacha.2006.11.037.

Ross, L., Valle-Levinson, A., Pérez-Santos, I., Tapia, F.J., Schneider, W. "Baroclinic annular variability of internal motions in a Patagonian fjord." *Journal of Geophysical Research: Oceans* 120.8 (2015): 5668-685. Web. 1 July 2017.

Ross, L., Pérez-Santos, I., Valle-Levinson, A., Schneider, W. "Semidiurnal internal tides in a Patagonian fjord." *Progress in Oceanography* 129 (2014): 19-34. Web.

Ross, L., Perez-Santos, I., Castro, L., Valle-Levinson, A. "Response of zooplankton abundance to internal motions and a glacial lake outburst flood in a Patagonian fjord: Zooplankton abundance in Patagonian." *2015 IEEE/OES Acoustics in Underwater Geosciences Symposium (RIO Acoustics)* (2015): n. pag. Web.

Ross, T. "A video-Plankton and microstructure profiler for the exploration of in situ connections between zooplankton and turbulence." *Deep Sea Research Part I: Oceanographic Research Papers*, vol. 89, 2014, pp. 1–10., doi:10.1016/j.dsr.2014.04.003.

Schlesinger, E. "The science of scientific writing — Judson Monroe, Carole Meredith, and Kathleen Fisher." *IEEE Transactions on Professional Communication* PC-21.2 (1978): 85. Web.

Sengupta, A., Carrara, F., Stocker, R."Phytoplankton can actively diversify their migration strategy in response to turbulent cues." *Nature*, vol. 543, no. 7646, 2017, pp. 555–558., doi:10.1038/nature21415.

Smith, W. O. "The seasonal cycle of phytoplankton biomass and primary productivity in the Ross Sea, Antarctica." *Deep Sea Research Part II: Topical Studies in Oceanography*, Pergamon, 12 Dec. 2000, www.sciencedirect.com/science/article/pii/S0967064500000618.

Somos-Valenzuela, M.A., Chisolm, R.E., Rivas, D.S., Portocarrero, C., Mckinney, D.C. "Modeling a glacial lake outburst flood process chain: the case of Lake Palcacocha and Huaraz, Peru." *Hydrology and Earth System Sciences* 20.6 (2016): 2519-543. Web.

Thompson, D. W. J., Barnes, E.A. "Periodic Variability in the Large-Scale Southern Hemisphere Atmospheric Circulation." *Science*, vol. 343, no. 6171, June 2014, pp. 641–645., doi:10.1126/science.1247660.

"Tortel Weather Forecast." *WorldWeatherOnline.com*, www.worldweatheronline.com/tortel-weather/aisen-del-general-carlos-ibanez-del-campo/cl.aspx.

US Department of Commerce, National Oceanic and Atmospheric Administration. *Ocean Today*, 5 July 2011, oceantoday.noaa.gov/fuelforthestorm/.

Valle-Levinson, A., Blanco, J.L. "Observations of wind influence on exchange flows in a strait of the Chilean Inland Sea." *Journal of Marine Research*, vol. 62, no. 5, Jan. 2004, pp. 720–740., doi:10.1357/0022240042387565.

Valle-Levinson, A., Cáceres, M.A. Pizarro, O."Variations of tidally driven three-layer residual circulation in fjords." *Ocean Dynamics* 64.3 (2014): 459-69. Web.

Valle-Levinson, A., Castro, A.T., De Velasco, G.G., Armas, R.G. "Diurnal vertical motions over a seamount of the southern Gulf of California." *Journal of Marine Systems* 50.1-2 (2004): 61-77. Web. 15 June 2017.

Valle-Levinson, A., Castro, L., Cáceres, M.A., Pizarro, O. "Twilight vertical migrations of zooplankton in a Chilean fjord." *Progress in Oceanography*, vol. 129, 2014, pp. 114–124., doi:10.1016/j.pocean.2014.03.008.

Valle-Levinson, A. "Definition and Classification of Estuaries." *Contemporary Issues in Estuarine Physics*, 2010. *Cambridge University Press*, doi:10.1017/cbo9780511676567.

Wilkinson, D. "Zooplankton-A lake's best friend." *Indiana Clean Lakes Program*, www.indiana.edu/~clp/documents/Zooplankton%20Factsheet.pdf.

Williamson, C.E., Fischer, J.M., Bollens, S.M., Overholt, E.P., Breckenridge, J.K. "Toward a more comprehensive theory of zooplankton diel vertical migration: Integrating ultraviolet radiation and water transparency into the biotic paradigm." *Limnology and Oceanography*, vol. 56, no. 5, 2011, pp. 1603–1623., doi:10.4319/lo.2011.56.5.1603.

Wooldridge, T., Erasmus, T. "Utilization of tidal currents by estuarine zooplankton." *Estuarine and Coastal Marine Science*, vol. 11, no. 1, 1980, pp. 107–114., doi:10.1016/s0302-3524(80)80033-8.

AUTHOR'S BIOGRAPHY

Brigitte Parady was born in Bar Harbor and attended Mount Desert Island High School in Mount Desert, Maine. Due to her academic achievements and impressive involvement in her community, she received the George Mitchell Scholarship Award to continue her education at the University of Maine at Orono. This prestigious scholarship is awarded to one graduating senior from every high school in Maine. Also through the efforts of George J. Mitchell, Brigitte received the George J. Mitchell Peace Scholarship to study abroad at the University College Cork in Cork, Ireland. Taking place in the spring of her junior year, this experience allowed her to establish an international reputation by presenting a group design for a refugee shelter to a representative of the United Nations. Following her study abroad experience, Brigitte returned to the University of Maine and conducted research under Professor Lauren Ross that was compiled into the accompanying Honors Thesis. Brigitte will graduate in May of 2018 with a Bachelor of Science degree.